CHALMERS

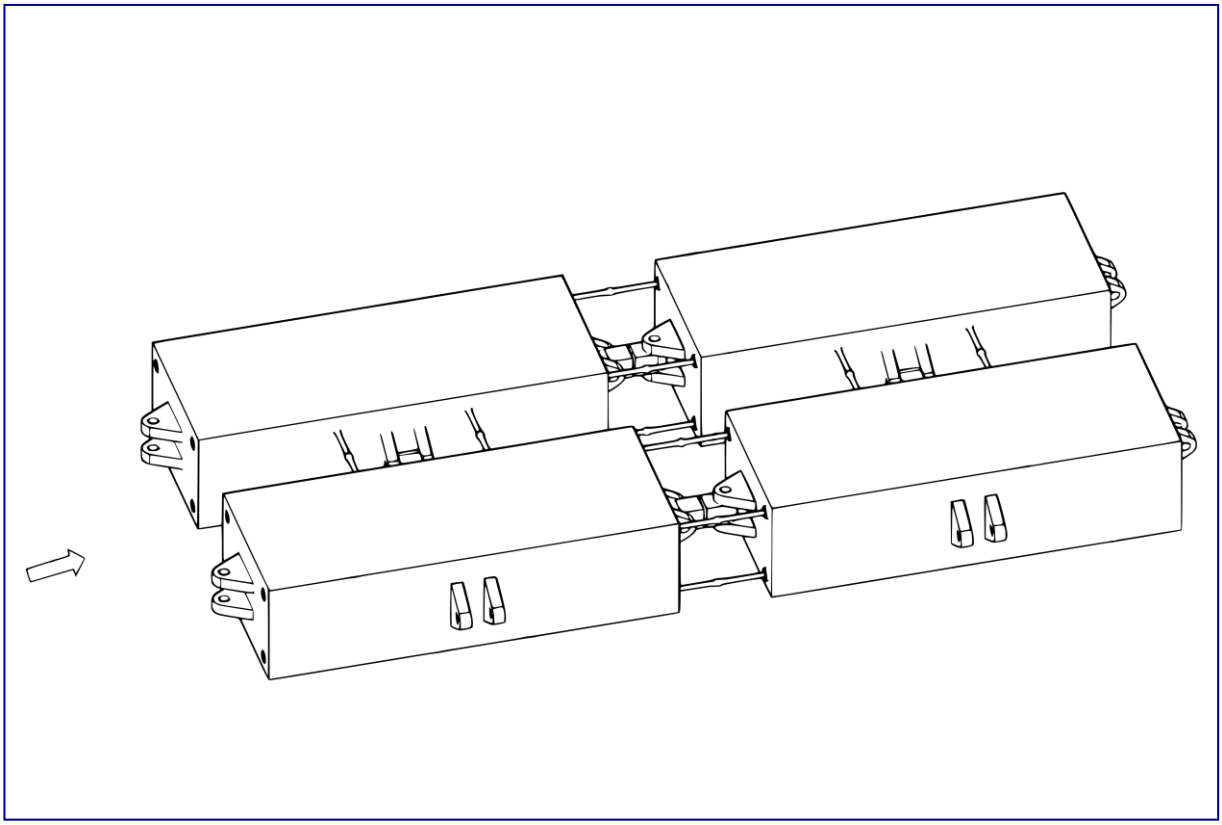

Design of a numerical model to analyse a wave energy dissipation device for hydropower

Master's Thesis within the Sustainable Energy Systems programme

FREDRIK HEDBERG

MICHAEL SACCULLO

Department of Applied Mechanics
Division of Fluid Dynamics
CHALMERS UNIVERSITY OF TECHNOLOGY
Göteborg, Sweden 2014
Master's thesis 2014:58

MASTER'S THESIS

Master's Thesis within *the Sustainable Energy Systems* programme

FREDRIK HEDBERG

MICHAEL SACCULLO

SUPERVISORS:

Professor ZHANG Yongliang

Professor Håkan Nilsson

EXAMINER

Professor Håkan Nilsson

Department of Applied Mechanics
Division of Fluid Dynamics
CHALMERS UNIVERSITY OF TECHNOLOGY
Göteborg, Sweden 2014

Master's thesis 2014:58

Design of a numerical model to analyse a wave energy dissipation device for hydropower

FREDRIK HEDBERG

MICHAEL SACCULLO

Master's thesis 2014:58

Master's Thesis 2014:58

ISSN 1652-8557

Department of Applied Mechanics
Division of Fluid Dynamics
Chalmers University of Technology
SE-412 96 Göteborg
Sweden
Telephone: + 46 (0)31-772 1000

Cover:
Suggested design for a wave energy dissipation device provided by Prof Zhang (Zhang, 2014).

Chalmers Reproservice
Göteborg, Sweden 2014
Master's thesis 2014:58

Design of a numerical model to analyse a wave energy dissipation device for hydropower

Master's Thesis in *the Sustainable Energy Systems* programme

FREDRIK HEDBERG

MICHAEL SACCULLO

Department of Applied Mechanics
Division of Fluid Dynamics
Chalmers University of Technology

ABSTRACT

Hydropower is a key technology for generating electricity. International goals of shifting to a more sustainable power production, elevates the future importance of this technology with low allocated emissions of greenhouse gases. Despite the long-term usage of hydropower, issues related to high wave energy level located in the stilling basin of the hydropower plant have not been given much attention earlier. One of these issues is the disturbance of nearby residents, mainly by infrasound pollution. The purpose of this thesis is to investigate the possibility to reduce wave energy in the outlet by a floating hinged-raft device. The suggested device will dissipate energy through interconnected piston dampers. The study is based on numerical simulations and the dissipation efficiency is to be calculated. Simplifications have been made throughout the investigation, hence the numerical simulations exclusively considers linear regular waves with an incident angle of zero. Six different samples with varying raft length and submerged area were investigated in order to find a satisfactory design. It has been found that the presented raft structure could dissipate wave energy significantly. It is recommended to optimize the design further and also broader the investigation area, e.g. simulate according to irregular wave theory, by introducing a mooring system and adding supplementary rafts in attempts to increase the dissipation efficiency.

Key words: Hydropower, infrasound, wave energy, linear wave theory, dissipation device, numerical simulations

Numerisk analys av en dissipationsanordning för vågenergi i vattenkraftsverk

Examensarbete inom masterprogrammet *the Sustainable Energy Systems*
FREDRIK HEDBERG
MICHAEL SACCULLO
Institutionen för Tillämpad mekanik
Avdelningen för Strömningsmekanik
Chalmers tekniska högskola

SAMMANFATTNING

Vattenkraft är en nyckelteknologi inom elproduktion i dagsläget. Internationella mål för att producera el mer hållbart medför att vattenkraft, med lågt allokerade växthusgasutsläpp, förväntas bli allt viktigare i framtiden. Dock har problem relaterade till hög vågenergi i utloppet av vattenkraftsanläggningar inte uppmärksammats märkbart tidigare, trots det långa nyttjandet av denna teknologi. Infraljud och övriga ljudföroreningar är ett av dessa problem som identifierats och drabbar boende i närheten av anläggningarna. Syftet med detta examensarbete är att undersöka möjligheten att reducera vågenergin i utloppet med hjälp av en flytande anordning med 2 ledade pråmar. Vågenergin dissiperas genom kolvdämpare som sammanlänkar anordningen och studien baseras på beräkningar av dissipationseffektiviteten genom numeriska simulationer. För att kunna ge ett första utlåtande är beräkningarna genomförda med förenklade antaganden såsom reguljär linjär vågteori. Dessutom genomfördes 6 olika fallstudier, där flottarnas längd och flytnivå undersöktes för att kunna föreslå en tillfredsställande design. Undersökningen visade på att det föreslagna konceptet kan reducera vågenerginivån i utloppet signifikant. Det är rekommenderat att undersökningarna ska utökas med simuleringar enligt irreguljär vågteori, inkludera förankringssystem och tillöka andelen pråmar för att förhoppningsvis förbättra dissipationseffektiviteten.

Nyckelord: Vattenkraft, Infraljud, vågenergi, linjär vågteori, dissipationsanordning, numeriska simulationer

Contents

ABSTRACT I

SAMMANFATTNING II

CONTENTS I

PREFACE III

ACKNOWLEDGEMENT IV

NOTATIONS V

1 INTRODUCTION 1

1.1 Hydro power 1

1.2 Problem description 3

1.3 Historical Background 4

1.3.1 Floating breakwaters 4

1.3.2 Wave energy converters 5

1.4 Objective 6

2 THEORETICAL BACKGROUND 7

2.1 Mechanical system of the rafts 8

2.2 Hydrodynamic equations 9

2.2.1 Continuity equation 9

2.2.2 Euler’s equation 10

2.2.3 Potential flow and incompressible fluid 11

2.3 Linearized wave theory 12

2.3.1 Superposition 13

2.3.2 Linearized boundary conditions for incident waves 13

2.3.3 Boundary conditions for fluid and structure interactions 16

2.4 Velocity potentials 17

2.4.1 Incident waves 17

2.4.2 Wave diffraction 18

2.4.3 Wave radiation 19

2.5 Hydrodynamic forces 20

2.5.1 Wave excitation force 20

2.5.2 Wave radiation forces 21

2.6 Motion of the wave energy dissipation device 23

3 METHOD 24

3.1 Assumptions/ Preconditions 24

3.1.1 Wave considerations 24

3.1.2 Deep water approximation 24

3.2 Evaluation measure 25

3.3 Computational tools 26
3.3.1 Calculation of Hydrodynamic forces in the frequency domain 26
3.3.2 Calculation of the device's motion response in time domain 27
3.4 Case definition 27
3.4.1 Investigation cases 28
3.5 Simulation procedure 29
3.5.1 Model definition for each sample 31
3.5.2 Parameter studies 33
3.5.3 Post-process 35

4 RESULTS AND DISCUSSION 37
4.1 Investigation of raft width, F2 37
4.1.1 Assessment of combined damping coefficient, F2 40
4.1.2 Assessment of wave period and wavelength, F2 41
4.1.3 Assessment of simulation gap, F2 44
4.2 Investigation of raft submerged area, M6 44
4.2.1 Assessment of raft submerged area to wave period, M6 46

5 GENERAL DISCUSSION 49
5.1 Result interpretation 49
5.2 Discussion of the numerical simulations 50
5.2.1 Comments about simulation gap 51
5.3 Further investigations 52

6 CONCLUSION 53

7 REFERENCES 54

8 APPENDIX A 56

9 APPENDIX B 59

Preface

In this thesis, a design concept of a wave energy dissipation device has been studied numerically. The device is developed for hydropower plant applications and is part of a research project conducted at the Department of Hydraulic Engineering, Tsinghua University in Beijing, China. The study was carried out between February to May 2014. Elforsk AB and the Program of Mechanical Engineering at Chalmers University of Technology financed the project, where Elforsk was the main financer. Supervisor at Tsinghua University was Professor Yongliang Zhang.

The report was carried out as a Master's thesis at the Division of Fluid Dynamics, Department of Applied Mechanics, Chalmers University of Technology, Sweden. Examiner of the thesis is Professor Håkan Nilsson.

Gothenburg, August 2014

Fredrik Hedberg

Michael Saccullo

Acknowledgement

We would like to thank the financiers, especially Elforsk AB that was the main founder of this project. Completing founding was obtained from the mechanical engineering program, program director Michael Enelund. Without this support this thesis would not be possible.

We are filled of gratitude to our supervisor Professor Yongliang Zhang, for the invitation and for all the essential guidance given to us along the way. This trip and project would not be possible without the appreciated commitment from Professor James Yang from Vattenfall R&D/KTH, making all necessary arrangements.

We would also like to acknowledge Wenchuang Chen and Siming Zheng for their help in both theoretical and practical difficulties, patience in discussion and the social activities making our stay more pleasant.

Professor Håkan Nilsson, our super visor at Chalmers, we owe gratitude for your valuable support and knowledgeable advises. Finally we would like to thank newfound friends in China, friends at home and our families.

Notations

Roman upper case letters

$\boldsymbol{C_{damp}}$	Damping matrix
$\boldsymbol{C_{rad}}$	Radiation resistance matrix
E_{wave}	Wave Energy [J]
$\dot{E}_{\mathrm{wave}}$	Wave Energy flux [J/m^{2}s]
F	Force [N]
H	Water height [m]
$\boldsymbol{K}$	Hydrostatic restoring force matrix
$\boldsymbol{N}$	Normal unit vector
$\boldsymbol{M_s}$	Structural mass matrix
$\boldsymbol{M_a}$	Added mass matrix
P	Power [W]
$P_{damping}$	Power dissipated by the dampers [W]
W	Work [J]
$\boldsymbol{U}$	Velocity field of the fluid
V	Volume [m^3]
S	Surface [m^2]
T	Wave period [s]

Roman lower case letters

a	Added mass
b	Combined damping coefficient [Ns/°]
c	Damping coefficient
c	Phase velocity of a wave
c_g	Group velocity of a wave
f	Frequency [Hz]
g	Standard gravity [m/s^2]
h	Water depth [m]
h_{barge}	Height of one barge/raft [m]
k	Wave number

Roman lower case letters (cont.)

k	Hydrostatic restoring force coefficient, spring coefficient [N/m]
l_{barge}	Length of one barge/raft [m]
$\boldsymbol{n}$	Outgoing normal unit vector of a surface
m	Mass [kg]
$\dot{\boldsymbol{m}}$	Mass flow [kg/s]
p	Pressure [N/m^2]
r	Radiation damping
s	Distance [m]
t	Time [s]
v	Velocity [m/s]

Greek lower case letters

η	Dissipation efficiency
$\eta\ (x,t)$	Vertical free-surface displacement of a wave [m]
λ	Wavelength [m]
θ	Rotational angle
θ_{rel}	Relative rotational angle [°]
$\dot{\theta}_{rel}$	Relative rotational angular velocity [°/s]
ρ	Density [kg/m^3]
ω	Vorticity
ω	Circular wave frequency
ϕ	Velocity potential

Mathmatical symbols

∇	Del operator
∇^2	Laplace operator

1 Introduction

The awareness of global warming being a global environmental challenge that needs to be faced by all nations increased during the last decades. Discussions are carried out on numerous levels in society, especially by the United Nations Intergovernmental Panel on Climate Change (IPCC). After the Fifth Assessment Report of the IPCC there is a scientific consensus that actions have to be taken sooner than later and to a greater extend then the actions carried out and planned today (Stocker, et al., 2013). Hydropower can play a key role for generating electricity in large quantities from a renewable energy source (IHA, 2000).

The Chinese government is facing environmental issues that are of local, regional and global concern such as global warming (NDRC, 2013). China has been one of the fastest growing economies during the last years and has become one of the largest economies in the world. The demand for energy increased along with the growing economy (Hu, Tan, & Xu, 2014). During this period of time many hydropower plants with large dams and volume flows were constructed (Han, Zhao, Dang, & Sun, 2009).

In October 2012 the Information Office of the State Council (SCIO) published a white paper on China's energy policy. The awareness and necessity of the environmental challenges have been acknowledged and an agenda has been developed to improve the situation for the people and the environment. Therefore, it was decided to enhance the position of hydropower in China, which already has grown to become the largest hydroelectricity producer in the world. The possibilities for exploiting hydropower are still comprehensive since the technically exploitable hydropower resources are currently utilized by less than 30 percent.

The SCIO formulated several goals to enhance sustainability that are to be achieved until 2020. At least 50 percent of the non-fossil energy consumption should be covered by the hydroelectric power generation, whereas the total share is supposed to be increased to 15 percent. In order to successfully accomplish this goal, more focus will be put on the construction of large hydropower structures at the main key rivers of the country. In addition, the damage to local and regional environment should be minimized. This ought to be pursued by implementing new regulations on ecological-protection. For instance an environmental-impact assessment is supposed to ensure the protection of the society within these regions. This ought not to be exclusively obligated for new built power plants, but also for already existing ones (SCIO, 2012). By acknowledging this, the foundation for this thesis is given.

1.1 Hydro power

Water reservoirs are created by damming up rivers and utilized as e.g. fresh water reservoir for drinking water or reservoirs for hydropower plants, which stores water with high potential energy. The potential energy is transformed into kinetic energy when water is flowing from the reservoir down to the basin or tail water area of a dam. The flowing water is utilized by a turbine in order to generate electricity. Because the water is channeled on different routes in and around a hydroelectric power plant, not all of it is used for the electricity production. The main route through the electricity generation division of a power plant into the stilling basin is presented in *Figure 1*.

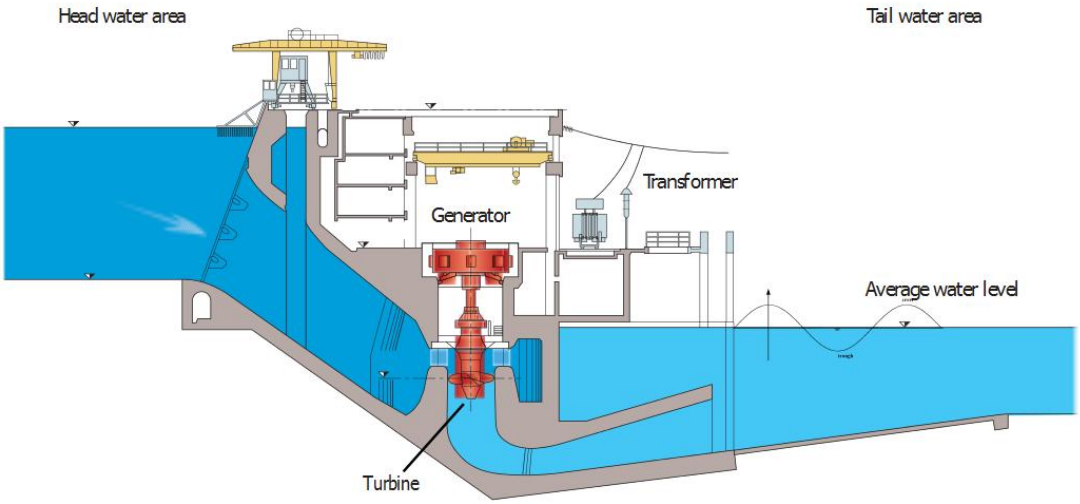

Figure 1 Sketch hydropower station (Verbund AG, 2007)

Another route to release water is through the spillway. An example is depicted in *Figure 2*. The purpose of a spillway is to discharge water from an overflowing reservoir into the stilling basin since every dam requires structures and facilities that guarantee a safe and controlled discharge possibility. This can be seen as a safety precaution within dam construction (Roberson, Cassidy, & Chaudhry, 1998).

The area of interest is the stilling basin at the bottom of the dam. Here interference waves, also called standing waves, may occur. Consequently energy dissipation structures are to put in place in order to minimize negative effects on the local environment. Another well-known effect due to the flow characteristics in the stilling basin is erosion, but also raising issues regarding freezing fog and spray from flip bucket jets that may encourage landslides. (Novak, Moffat, Nalluri, & Narayanan, 2007).

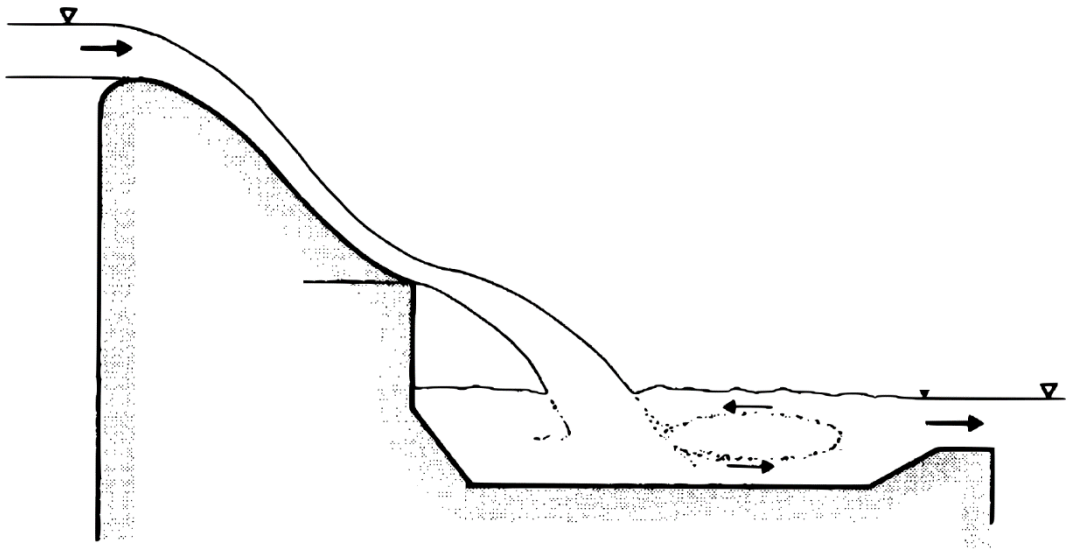

Figure 2 Sketch high-head spillway (Novak, Moffat, Nalluri, & Narayanan, 2007)

1.2 Problem description

The main concern directly related to this work is waves with high energy levels in the stilling basin. This is illustrated in *Figure 1*. The structural integrity of the dam and stilling basin are directly affected and can additionally cause issues regarding erosion and sound pollution. Erosion can cause severe damage to the local environment and attached ecosystems. Land degradation, increased sedimentation of water reserves, loss of nutrients, and accumulations of chemical particles are some of the problems recognized by this effect (Toy, Foster, & Renard, 2002). Sound pollution affects the local environment by disturbing nearby residents, but no thorough investigation has taken place according to Prof. Zhang. The main concern regards sound waves with very low frequency, even undetectable for the human ear. The so-called infrasound may cause vibrations in and around these settlements and thereby interferes with the residents' everyday life. These effects already occur today and might even be amplified with increasing size of a hydropower plant (Zhang, 2014).

In order to reduce impacts related to high water energy levels a suggested solution is to place one-way hinged floating energy dissipation devices in the basin. Hydraulic dampers connecting the rafts as shown in *Figure 3* dissipates the wave energy. The arrow marks the incoming wave direction.

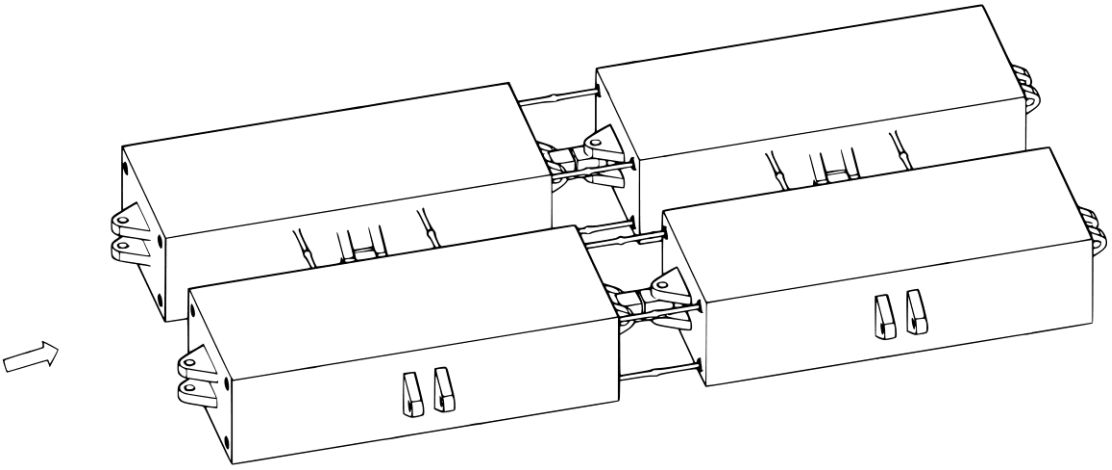

Figure 3 Double-hinged floating rafts (Zhang, 2014)

This wave energy dissipation device is to be further examined in this master thesis. Emphasis will be given to investigate the dissipation efficiency and its relation to the characteristics of water waves. The investigation will be based on mathematical models of fluid-structure interaction and studies are performed by using numerical software. As no research is to be found on this specific topic there is a need to start with simplified models, e.g. only regular waves are to be considered (Zhang, 2014).

1.3 Historical Background

The presented double-hinged floating is related to a hinge-barge system, which has proven to be very useful for several different fields and application. According to Kraemer bridges and piers were the earliest applications. Nowadays hinged-barge systems are also utilized for loading and unloading ships, produce fresh water, and converting wave energy (Kraemer, 2001). The theoretical winnings in the analysis of hinged-barge systems have mainly been driven by the ocean engineering field concerning deep-draft ship accommodation and more recently energy harvesting devices (McCormick, 1987). These seemingly unrelated areas have suggested the hinged barge system as a potential key technology in both reducing and harvest wave energy.

In this thesis a historical background of the development of some wave energy applications will be presented. The reduction of wave energy and in particular protection against demolishing wave forces is reviewed in the first subchapter, floating breakwaters. This includes the progress of vessel accommodation, settlement protection and the loading and unloading of ships. The increased importance of renewable energy sources has given attention to harvest useful energy from ocean waves, hence hinged-barged systems became of renewed interest. A brief introduction to general ocean energy converters and especially the hinged-barge concepts is presented in Subchapter 0.

Stated earlier, this thesis will not include energy harvesting applications, where the energy is converted into more useful forms. The emphasis will be on dissipating wave energy in an effective way. With this said, the related research regarding general behavior of hinged barge systems is of great importance.

1.3.1 Floating breakwaters

In order to shelter ships and settlements, artificial constructions protecting against waves, winds and currents have been built long throughout history. It is suggested that structures for this purpose have been made since the 13th century by the Phoenicians. With the objective to improve transport of people and cargo or to conserve and reclaim land, different approaches have been presented to ensure calm water inshore. Breakwaters permanently fixed on the seabed are mostly used today. They are often of considerable mass and size in order to operate effectively and withstand the mechanical forces related to the waves. The breakwater constitutes a structure where the wave energy is to be reduced, either by absorption or deflection (Encyclopædia Britannica, 2014).

Breakwaters constructed without being permanently fixed were not given much attention until the Second World War. At that period of time new transportable devices was introduce to enable safe unloading of soldiers and material. During the invasion of Normandy two new types were tested on large scale; the portable barge type that sunk into a stable position once filled with water, and a free-floating breakwater kind. Both designs were satisfactory. The free-floating type collapsed however in the event of an unexpected storm largely exceeding the design conditions. When U.S. Navy Civil Engineering Laboratory in 1957 started investigating the potential for shelter small boats for safe anchorage enabling cargo transfer maneuvers, the floating breakwaters gained a lot of attention. Since then a large amount of variations of this kind of floating configuration have been designed (Hales, 1981).

Floating breakwaters seem especially suitable for small harbors with few crafts anchorages, where the economic costs and environmental modifications using permanently fixed breakwaters cannot be justified (Hales, 1981). Fixed breakwaters might not even be an option at locations with poor foundation conditions. Additionally the expenses are high for bottom-connected structures where the water is deep. Other beneficial properties with the floating device are for instance the movability so the structure can easily be rearranged or removed in order to avoid damage connected to ice formation. Floating breakwater is also favorable when water-quality, water circulation and fish mitigation is of concern due to low interference to local environment. (McCartney, 1985).

Numerous amounts of floating breakwaters have been proposed and the methods applied to reduce wave energy include reflection, dissipation, interference and conversion. Common for all concepts is the requirement of a mooring system and that the configuration needs to be designed for the local conditions where it is to operate. Disadvantages connected to the floating configuration are mainly related to the performance. The permanently fixed breakwaters generally give better protection and the wave energy reduction is easier to predict (Hales, 1981). A fundamental problem is the inevitable slack in the moorings, especially at locations with high tide range. The slack might cause the breakwaters to ride on long waves without effectively reduce the transmitted wave energy onto the protected area (Encyclopædia Britannica, 2014).

1.3.2 Wave energy converters

The vast energy in ocean waves has been investigated for a long time in order to extract useful energy, which has given rise to many different concepts. Many methods are applied and can be floating, mounted to the seabed or both. Li and Yu summarize the history of ocean wave energy converters and also present the categories these prototypes can be assigned to. These categories are oscillating water columns, point absorbers, overtopping systems, and bottom-hinged systems (Li & Yu, 2012). This thesis will give special focus to floating-pitching devices, described below.

Systems that harvest useful energy by the relative motions of hinged barges due to excitement of wave energy are the Hagen-Cockerell rafts. Actually Hagen and Cockerell developed their systems independently; Hagen developed the *Wave driven generator* and Cockerell named his invention the *Apparatus for extracting energy from wave movement at the sea* (Hagen, 1976) (Cockerell, 1978). The resemblances in the inventions however made Hagen-Cockerell the general term for several floating wave energy converters, based on this hinged barge methodology (Kraemer, 2001). Other variations of the system are to be found, e.g. McCabe's *Wave powered mover* (McCabe, 1991). The prototypes differentiate for example in design to function in an altered wavelength span and have different stability requirements. Further, Kraemer also discusses an application that could both generate electricity and produce fresh water by a reverse-osmosis process, which is called the McCabe Wave Pump (Kraemer, 2001).

Various types of floating hinged-barge systems have been developed and recently have many of them been designed for energy-harvesting. The floating hinged barge system has proven to effectively capture wave energy with high efficiency and high reliability.

Almost all previous studies on raft type wave energy devices have been focusing on absorbing and then converting wave energy to more useful forms of energy. In most of the studies, the considered prototypes convert wave energy into hydraulic energy, which is used in different hydraulic motors to gain mechanical power or to generate electricity. Hinge barged systems designed for dissipating wave energy is however barely mentioned (Zhang, 2014).

McCartney discusses how the investigations formerly have been restricted to smaller single floating structures, designed to provide shelter from small or intermediate waves in areas such as lakes, reservoirs, rivers and estuaries that are semi protected. Furthermore McCartney reasons how the prospects of reducing larger waves and other applications should be investigated when further research is employed to larger structures and multiple joint floating breakwaters (McCartney, 1985).

1.4 Objective

The purpose of this thesis is to investigate how incident wave characteristics influence the energy dissipation efficiency of a wave energy dissipation device. The wave energy dissipation device is assessed of utilisation in the stilling basin of hydropower plants to reduce the wave energy in the outflow, causing problems with structural mechanical stresses and local environmental issues. The investigation will be based on numerical studies, and the parameters to be considered is wave height, wave length and wave period. A mathematical model of water waves is to be designed to simulate the flow characteristics. The performance of the device is evaluated by using numerical software with focus on solid and fluid interactions for maritime applications.

The analysis will be based on simplified cases where water waves will be treated as linear, regular waves with an incidence angle of zero. These assumptions are carried out to make a scientific statement about the performance within a limited time period and available computer resources. The focus of this study is to design a model for evaluating the dissipation efficiency. Economical, constructional or other aspects are not taken into account in this thesis to evaluate if this type of device is suitable or not for hydropower plants.

2 Theoretical Background

This chapter describes the investigated system in order to perform the numerical analysis, both mechanically and mathematically. At first a mechanical system representing the rafts is presented. It has to be pointed out that this is done very briefly. The rafts are interconnected through dampers and are driven by the external forces induced by the incident waves. The influence of these forces can be found later in this chapter.

The calculations are carried out in a three dimensional system resulting in 6 degrees of freedom for each raft. In this work movements around the y-axis are however of the greatest interest. For illustration purposes the raft system is shown in the z-x-plane only. For this investigation of energy dissipation focus will be on the directions called surge, heave and pitch, pictured in *Figure 4*. Other movements will not be neglected, but as the incoming waves move in x-direction and perpendicular to y- and z-direction, are the rafts consequently mostly excited in these modes. Additionally are the wave characteristics assumed to be linear and Airy's linear wave theory is applied for their determination. However, the equations of motion can become of non-linear character.

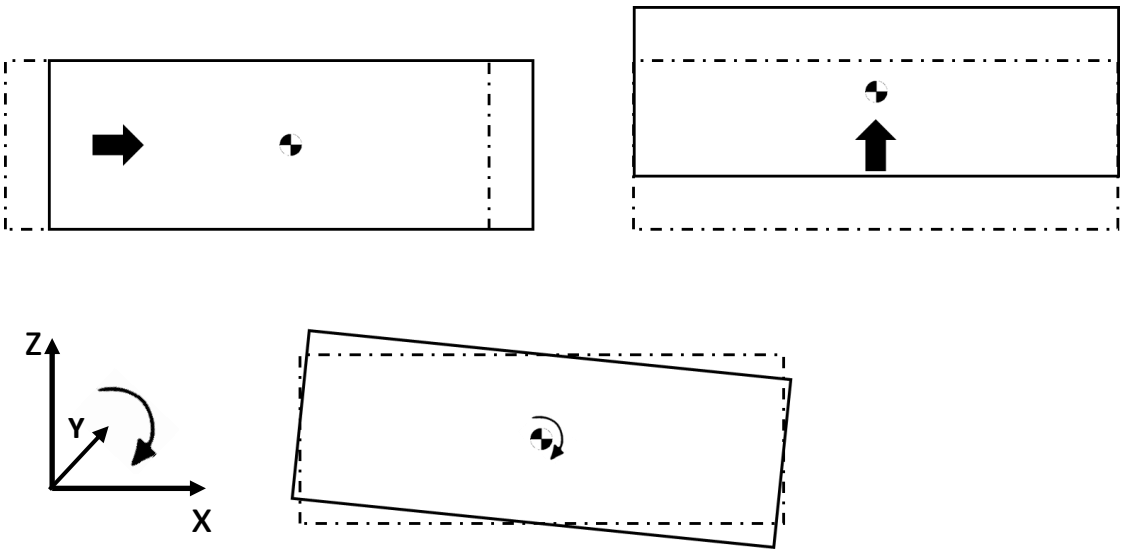

Figure 4 *Surge, heave and pitch movements of a raft*

Surge is a longitudinal translation in x-direction. Heave is a linear vertical translation in z-direction and pitch as a rotation about its transverse axis. The complicated fluid-structure interactions make it difficult to predict the motion of the energy dissipation devices, which is induced by water waves at the stilling basin of hydro power plants. The numerical software AQWA LINE can be used to simulate non-linear problems, but a discussion where and to what extend non-linearity will be used in the simulation is held in Chapter 3.3.

2.1 Mechanical system of the rafts

The investigated system is constituted of two raft connected by a hinge and dampers. The configuration is presented in *Figure 5*. The system geometry is the basis for all calculations conducted in this paper. Raft one and two are equal of length (l_{raft}), but the dimensions can differ for different designs. A detailed explanation will follow in Chapter 3. The linear dampers are placed as pictured, but for simplicity reasons not drawn in the following sketches.

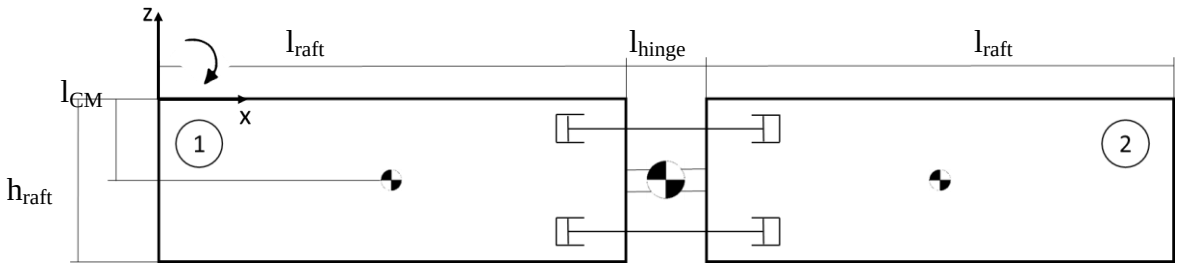

Figure 5 Hinged raft system

The length of the hinge (l_{hinge}) is neglected and the raft height (h_{raft}) can be seen as small compared to the length.

As mentioned before, the hinged rafts have 3 relevant degrees of freedom in the vertical plane. Because the energy dissipated through the dampers is to be calculated, the relative rotational velocity around the hinge is of greatest interest. The energy dissipated in the connection of the mechanical system is directly related to the dissipated wave energy. The waves also constitute the external forces acting on the rafts.

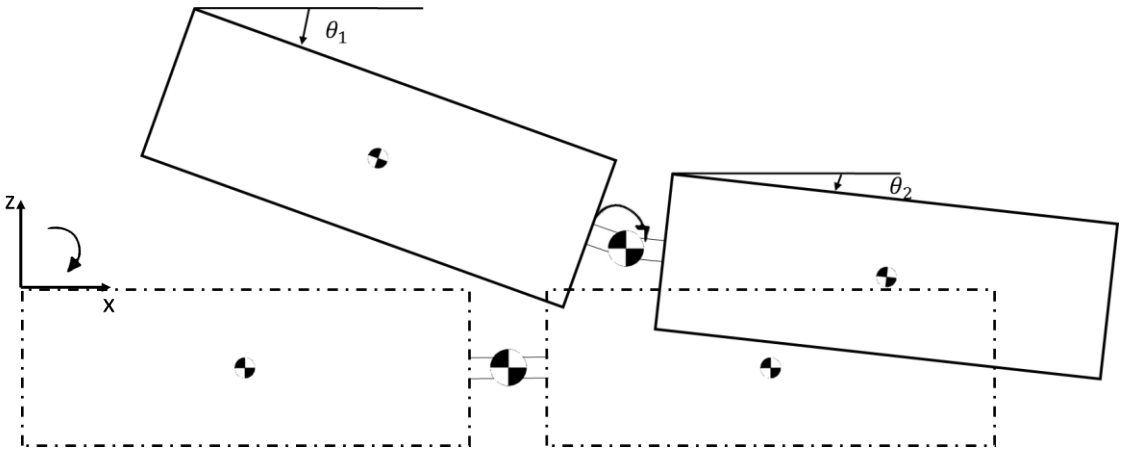

Figure 6 Displacement of the whole system

$$\theta_{rel}(t) = \theta_1(t) - \theta_2(t) \tag{2.1}$$

$$\dot{\theta}_{rel}(t) = \dot{\theta}_1(t) - \dot{\theta}_2(t) \tag{2.2}$$

The equation above states the relative rotational angle, $\theta_{rel}(t)$, and the relative angular velocity, $\dot{\theta}_{rel}(t)$, both around the y-axis. The angular velocity is of great importance in order to calculate the energy dissipated through the dampers. Hence the dissipation efficiency can be calculated. In order to show how the kinematics of the rafts is related to the energy dissipation efficiency, the equations are briefly discussed here. More details are found in Subchapter 3.2.

The dissipated energy in the waves is calculated by the power dissipated in the dampers. The power *P* is given in the following equations.

$$P = \frac{W}{t} = \frac{Fs}{t} = Fv = [cv] * v \tag{2.3}$$

As a result one can state that *P* equals the damping coefficient *c* times the velocity squared. This is not only true for linear dampers, but also for rotational dampers when using the rotational angular velocity.

$$P_{damping} = \left(b * \dot{\theta}_{rel}^2\right) \tag{2.4}$$

Where *b* is a combined damping coefficient and $\dot{\theta}$ represents the relative angular velocity, in the means of the subtraction of the two angular velocities of each raft. The combined damping coefficient is particularly used in combination with the angular velocity.

The next subchapter covers the calculation of the external forces on the basis of linear wave theory.

2.2 Hydrodynamic equations

Water waves are well studied within many areas, such as in ocean engineering, fluid dynamics and naval architecture. In this chapter a method used to simulate the flow of the fluid is presented. The assumptions made to greatly simplify the given case are also derived. The hydrodynamics equations describing the flow are based on basic fluid dynamics and are used for solving the forces of the waves inducing motion of the rafts. A fluid's density, pressure and velocity field are sufficient properties to describe the flow for this problem. The basic governing equations are the continuum equation combined with Newton's second law of motion, which will under the given assumptions formulate the fundamental expression for linearized wave theory.

2.2.1 Continuity equation

The continuity equation states the conservation of mass and is derived in following steps. The fluids' mass flow is,

$$\dot{\boldsymbol{m}} = \rho \boldsymbol{U} \tag{2.5}$$

Where ρ is the fluid density and the velocity field vector **U** is described by the unit vectors:

$$\boldsymbol{U}(x, y, z) = u\boldsymbol{i} + v\boldsymbol{j} + w\boldsymbol{k} \tag{2.6}$$

Additionally, is the del operator defined for Cartesian coordinates system (McCormick, 2010).

$$\nabla = \frac{\partial}{\partial x}\boldsymbol{i} + \frac{\partial}{\partial y}\boldsymbol{j} + \frac{\partial}{\partial z}\boldsymbol{k} \tag{2.7}$$

Methods to derive the hydrodynamic equations are presented in (Persson, 2014) and start with the equation for the change in mass in a volume *V* per unit time:

$$\frac{\partial}{\partial t}\int_V \rho \, dV = \int_V \frac{\partial \rho}{\partial t} \, dV \tag{2.8}$$

The change in mass could also be expressed by using the Gauss divergence theorem. If no mass is consumed or produced within the volume and *S* equals the enclosing area of *V*, then:

$$-\int_S \rho \boldsymbol{U} \, dS = -\int_V \nabla \cdot (\rho \boldsymbol{U}) \, dV \tag{2.9}$$

By combine the two expressions, it is given:

$$\frac{\partial \rho}{\partial t} + \nabla \cdot (\rho \boldsymbol{U}) = 0 \tag{2.10}$$

If the fluid is incompressible this state changes in density can be neglected:

$$\frac{\partial \rho}{\partial t} = 0, \nabla \rho = 0 \;\rightarrow\; \nabla \cdot (\boldsymbol{U}) = 0 \tag{2.11}$$

2.2.2 Euler's equation

Secondly, the motion of the conservation of momentum of the fluid is to be described. According to Persson, the momentum for the volume *V* is:

$$\int \rho \boldsymbol{U} \, dV \tag{2.12}$$

The volume's momentum is either changed by the excitement of external forces or by momentum flux through the surface S. If the surface element dS is to be considered, then the momentum $\rho \boldsymbol{U}$ flowing out equals $\rho \boldsymbol{U}\boldsymbol{U} \, dS$. Total momentum flux out of the volume *V* is therefore:

$$\oint_S \rho \boldsymbol{U}\boldsymbol{U} \, dS \tag{2.13}$$

External forces that might act on the system are i.e. the gravitational force. In order to derive Euler equation, Persson assumes the external forces are limited to the arising pressure. The force applied to the system equals:

$$-\oint_S p \cdot dS \tag{2.14}$$

Another necessary assumption is to neglect the viscosity when formulating Euler equation. If viscosity were included in the expression above, this would equal Navies Stokes equations. Total change of momentum per time unit according to Euler becomes:

$$\frac{\partial}{\partial t}\int(\rho \boldsymbol{U})\,dV = -\oint_{\boldsymbol{S}}(\boldsymbol{\rho U U})\cdot dS - \oint_S p\cdot dS$$

$$= -\int_V \nabla\cdot(\rho \boldsymbol{U U})\,dV \; -\int_V \nabla\cdot p\,dV = \int_V\{-\nabla\cdot(\rho \boldsymbol{U U}) - \nabla p\}\,dV$$

$$\rightarrow \frac{\partial}{\partial t}(\rho \boldsymbol{U}) = -\nabla\cdot(\rho \boldsymbol{U U}) - \nabla p \tag{2.15}$$

Combining Euler's equation with the continuity equation formulated above following expression appears:

$$\frac{\partial}{\partial t}(\rho \boldsymbol{U}) = \rho\frac{\partial \boldsymbol{U}}{\partial t} + \boldsymbol{U}\frac{\partial \rho}{\partial t} = \rho\frac{\partial \boldsymbol{U}}{\partial t} - \boldsymbol{U}\boldsymbol{\nabla}\cdot(\rho \boldsymbol{U})$$

$$\rightarrow \rho\left(\frac{\partial \boldsymbol{U}}{\partial t} + \boldsymbol{U}\cdot\boldsymbol{\nabla U}\right) = -\boldsymbol{\nabla} p \tag{2.16}$$

2.2.3 Potential flow and incompressible fluid

Stated earlier, a fluid is considered incompressible when the density is constant. To describe the velocity field and pressure field, the described functions above are applied. With the incompressible fluid assumption the continuity equation then becomes $\nabla\cdot(\boldsymbol{U}) = 0$, and correspondingly the Euler equation is then:

$$\frac{\partial \boldsymbol{U}}{\partial t} + \boldsymbol{U}\cdot\boldsymbol{\nabla U} = -\boldsymbol{\nabla}\left(\frac{p}{\rho}\right) \tag{2.17}$$

By using the relation:

$$\nabla\left(\frac{\boldsymbol{U^2}}{2}\right) = (\boldsymbol{U}\cdot\boldsymbol{\nabla})\boldsymbol{U} + \boldsymbol{U}\times(\boldsymbol{\nabla}\times\boldsymbol{U}) \rightarrow (\boldsymbol{U}\cdot\boldsymbol{\nabla})\boldsymbol{U}$$

$$= \nabla\left(\frac{\boldsymbol{U^2}}{2}\right) - \boldsymbol{U}\times(\boldsymbol{\nabla}\times\boldsymbol{U}) \tag{2.18}$$

The Euler equation is reformulated to:

$$\frac{\partial \boldsymbol{U}}{\partial t} + \boldsymbol{\nabla}\left(\frac{\boldsymbol{U^2}}{\boldsymbol{2}}\right) - \boldsymbol{U}\times(\boldsymbol{\nabla}\times\boldsymbol{U}) = -\boldsymbol{\nabla}\left(\frac{p}{\rho}\right) \tag{2.19}$$

To introduce the vorticity of the velocity field, first the definition of the curl is given for a general vector field **F**. The vorticity is the curl of a velocity field.

$$Curl\ of\ vector\ field\ \{\boldsymbol{F}\} = \nabla\times\boldsymbol{F}$$
$$Vorticity\colon \omega = \nabla\times\boldsymbol{U}$$

By applying the curl to both sides of the Euler equation and in the second step substitute with the vorticity, following expression is specified.

$$\nabla\times\left\{\frac{\partial \boldsymbol{U}}{\partial t} + \boldsymbol{U}\cdot\boldsymbol{\nabla U}\right\} = \boldsymbol{\nabla}\times\left\{\boldsymbol{\nabla}\left(\frac{p}{\rho}\right)\right\} \tag{2.20}$$

$$\frac{\partial \omega}{\partial t} - \nabla\times(\boldsymbol{U}\times\boldsymbol{\omega}) = 0 \tag{2.21}$$

When the flow is assumed to be irrotational the vorticity is by definition 0 (Kraemer, 2001), giving

$$\omega = \nabla \times \boldsymbol{U} = 0 \tag{2.22}$$

If the velocity field is of such is can be represented by a gradient of a scalar function, this will be one possible solution to satisfy this equation. The scalar function is called the velocity potential, Φ.

$$\boldsymbol{U} = -\boldsymbol{\nabla\phi} \tag{2.23}$$

The velocity potential can be used and only used when the flow is irrotational (McCormick, 2010). Referring back to the equation of continuity for incompressible flow and applying the velocity field results in following expression.

$$\boldsymbol{\nabla \cdot U = \nabla \cdot \nabla\phi = \nabla^2\phi = 0} \tag{2.24}$$

The ∇^2 is also referred to as the Laplacian, defined by (McCormick, 2010):

$$\boldsymbol{\nabla^2} = \frac{\partial^2}{\partial x^2} + \frac{\partial^2}{\partial y^2} + \frac{\partial^2}{\partial z^2} \tag{2.25}$$

Under the assumptions of irrotational, incompressible flow, it is concluded that the Laplace equation $\boldsymbol{\nabla^2\phi} = 0$ and the scalar function Φ must satisfy this condition everywhere in the fluid domain. The Laplace equation is the fundamental equation of linearized wave theory and is also referred to the linearized equation for continuity of irrotational flow. Linearity is obtained by representing the velocity field by 1 dependent variable Φ instead of 3:

$$\boldsymbol{U} = u\boldsymbol{i} + v\boldsymbol{j} + w\boldsymbol{k} = \frac{\boldsymbol{\partial\Phi}}{\boldsymbol{\partial x}}\boldsymbol{i} + \frac{\boldsymbol{\partial\Phi}}{\boldsymbol{\partial y}}\boldsymbol{j} + \frac{\boldsymbol{\partial\Phi}}{\boldsymbol{\partial z}}\boldsymbol{k} \tag{2.26}$$

As mention earlier it is sufficient to know the fluids density, pressure and velocity field to describe the flow under these assumptions. According to McCormick whom included gravity forces, the irrotational form of Euler equation becomes:

$$\boldsymbol{\nabla\rho}\left(\frac{\partial\phi}{\partial t} + \frac{\boldsymbol{U^2}}{\boldsymbol{2}} + gz + \frac{p}{\rho}\right) = 0 \tag{2.27}$$

The second fundamental equation in the linearized wave theory is the Bernoulli's equation, describing the conservation of energy for irrotational flows. The equation is obtained by spatial integration of the irrotational Euler equation hence a time function, $f(t)$, appears on the right hand side.

$$\boldsymbol{\rho}\frac{\partial\phi}{\partial t} + \rho\frac{\boldsymbol{U^2}}{\boldsymbol{2}} + \boldsymbol{\rho}gz + p = f(t) \tag{2.28}$$

2.3 Linearized wave theory

Airy's linear wave theory, also known as linearized wave theory, is a basic way of describing the wave phenomena. Even though it might seem to be simplified to a great extent, the theory corresponds quite well to observed results. This is especially true for systems with a small ratio between the wave height and wavelength (McCormick, 2010). In previous section the nonlinear Euler equation is linearized under the

irrotational flow formulation of the equation. If and only if these conditions apply, the velocity field may be represented by a gradient to the scalar function.

For an irrotational, incompressible flow the equation for continuity results in the Laplace equation which is fundamental for linearized wave theory. For this the scalar function of the Laplace equation must be satisfied everywhere in the fluid domain. The Laplace equation describes the wave phenomena by a second order linearized equation; hence the equation has a general and particular solution. Fundamental in the Airy linearized wave theory is that the particular solution is calculated by the utilization of linearized boundary conditions, described in the sections below (McCormick, 2010).

Firstly however the properties of a linearized flow will be investigated further and the fundamental super positions principle will be described, stating how different wave phenomena can be treated separately and solved with a respective velocity potential.

2.3.1 Superposition

The principle of superposition allows the solid-fluid interaction of a floating object to be divided into three different problems, namely; incident waves, wave diffraction and wave radiation. Diffraction describes how the velocity field is changed in presence of a rigid fixed body. Radiation regards the changes due to an oscillating body in the absence of incident waves. Each of these effects can be expressed with linearized equations through the utilization of linearized wave theory. Furthermore, these sub problems can be solved independently with a velocity potential, which was done for the incident wave equation above. The principle of superposition states the individual velocity potentials can be summarized in order to obtain a particular solution for the flow. In the whole fluid domain the Laplace equation must be valid. The added velocity potential is hereon called the total velocity potential and is given in equation below (Kraemer, 2001).

$$\phi_{total} = \phi_0 + \phi_{dif} + \phi_{rad} \tag{2.29}$$

ϕ_{total} represents the added velocity potential, ϕ_0 is the potential for incident waves, ϕ_{dif} is the potential solving the diffraction problem and ϕ_{rad} is the radiation velocity potential. The different velocity potentials are further explained in Subchapter 2.5**.**

2.3.2 Linearized boundary conditions for incident waves

In this section the linearized boundary conditions are presented and used according to Airy linearized wave theory to derive the velocity potential for incidence waves. There are three boundary conditions, each one presented in own subchapter. Finally they will be combined to obtain the linearized free surface condition, presented in Subchapter 2.4**.**

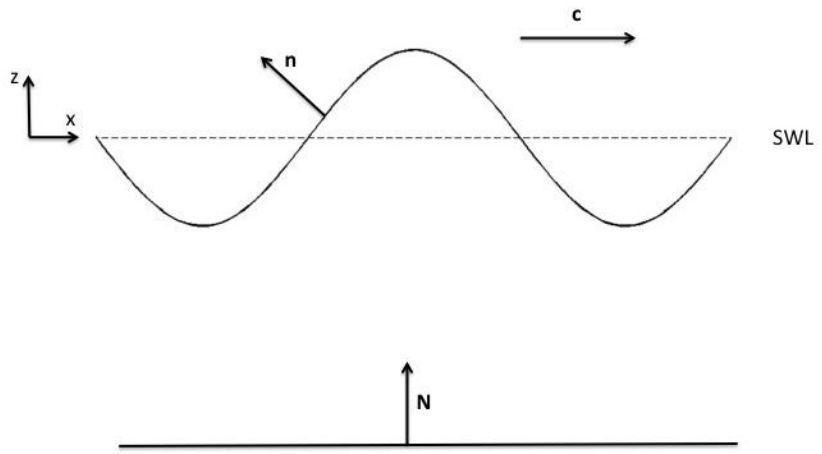

Figure7 Schematic view of wave characteristics.

2.3.2.1 Kinematic free surface condition

This boundary condition states that the particles on the free surface of the wave are required to have the identical velocity as the free surface at all times. Consider a function of the vertical free-surface displacement of the wave- $\eta(x,t)$, which will be dependent on time, t, and distance in x-direction. The displacement is evaluated as the distance from still water line; see *Figure 8* for further details.

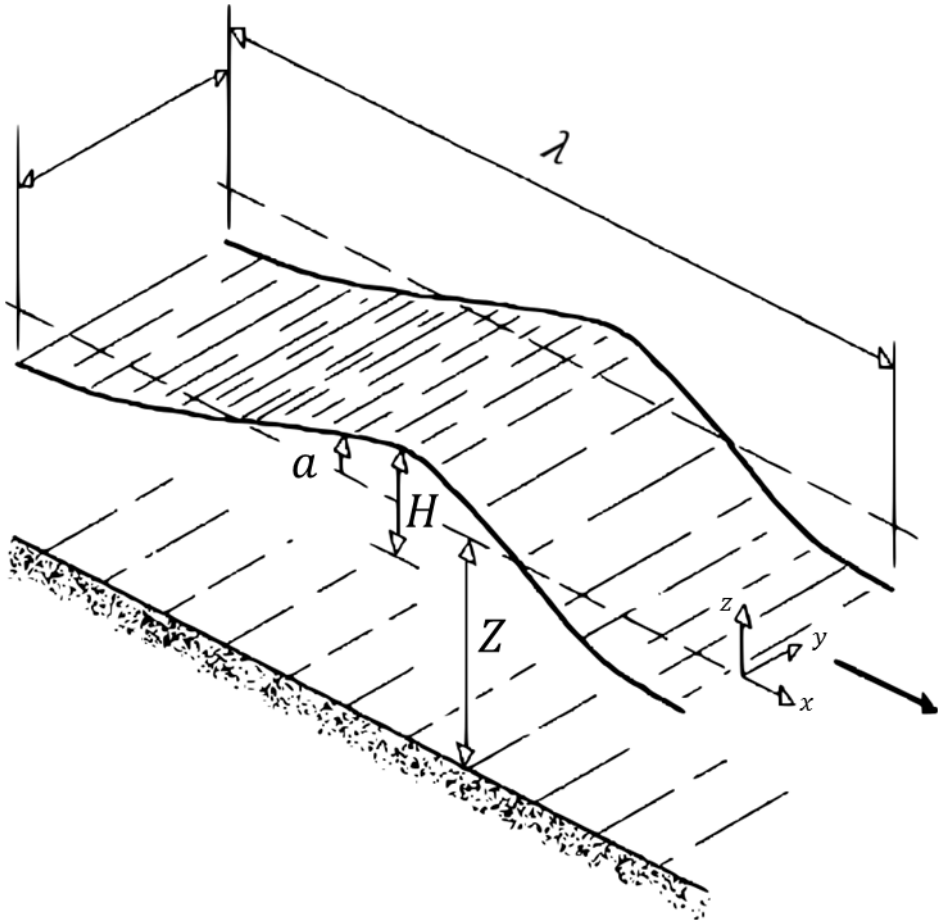

Figure 8 Schematic view of notation of wave characteristics

The kinematic free surface condition gives the velocity field of particles at the free surface, mathematically be expressed by:

$$\boldsymbol{U}|_{\boldsymbol{z=\eta}} = \boldsymbol{U_n} \tag{2.30}$$

Where **n** is the unit normal vector pointing out from the free surface, see *Figure7*. Assuming irrotational flow, the equation yields:

$$\boldsymbol{U}|_{\boldsymbol{z=\eta}} = \boldsymbol{\nabla\phi}|_{\boldsymbol{z=\eta}} = \boldsymbol{n}\frac{\boldsymbol{\partial\phi}}{\boldsymbol{\partial n}}\Big|_{\boldsymbol{z=\eta}} \tag{2.31}$$

Following approximation of the boundary condition is applied if the vertical displacement is small compared to the wavelength, $\frac{\eta}{\lambda} \ll 1$,

$$\boldsymbol{U}|_{\boldsymbol{z=\eta}} \cong \frac{\partial\eta}{\partial t}\boldsymbol{k} \cong \frac{\partial\Phi}{\partial z}\Big|_{\boldsymbol{z=0}}\boldsymbol{k} \tag{2.32}$$

It is important to distinguish between the two terms, as $\frac{\partial\eta}{\partial t}\boldsymbol{k}$ is employed at the free surface, $z = \eta$, and $\frac{\partial\Phi}{\partial z}\Big|_{\boldsymbol{z=0}}\boldsymbol{k}$ is applied at the still water line, $z = 0$ (McCormick, 2010).

2.3.2.2 Sea-floor condition

This condition states the sea floor is to be evaluated as a solid surface, with no movement across the boundary. Referring to *Figure **8*** once again, the sea floor is located uniformly at $z = -h$, where h is the water depth and **N** is the normal unit vector to the seafloor. According to McCormick the sea-floor boundary condition is then formulated as

$$\boldsymbol{U}\cdot\boldsymbol{N}|_{\boldsymbol{z=-h}} = \frac{\partial\Phi}{\partial N}\Big|_{\boldsymbol{z=-h}} = 0 \tag{2.33}$$

2.3.2.3 Dynamic free surface condition

This boundary condition states that for any position x and any time t at the free surface, the pressure gauge is zero. Due to the irrotational flow equation the pressure can be obtained in the whole fluid domain by Bernoulli equation.

$$\boldsymbol{\rho}\frac{\partial\phi}{\partial t} + \rho\frac{\boldsymbol{U^2}}{\boldsymbol{2}} + \boldsymbol{\rho}gz + p = f(t) \tag{2.34}$$

First a case when no wave excites the water, called still water condition, is considered. The Bernoulli equation is then reduced only to the last two terms on the left hand side, because no wave motion is present.

The free surface is uniformly located at $z = 0$, due to no water waves. The gauge pressure at this surface is also zero, as the dynamic free surface boundary condition is applied. Hence the time function will also be equal to zero $f(t) = 0$. Still water can also be formulated as a wave with an infinite wavelength and no wave height. If the time function is zero for one wave, $f(t) = 0$, this equality must be satisfied for all waves.

The dynamic free surface condition is now formulated for cases were the water height H and wavelength λ is finite.

$$\left\{\frac{\partial \phi}{\partial t} + \frac{U^2}{2} + g\eta\right\}\Big|_{z=\eta} = 0 \tag{2.35}$$

This is a non-linear equation due to the velocity term is of empowered by 2. To linearize this equation, waves with small wave steepness ($\lambda >> H$) is to be considered. The squared velocity term describing the kinetic energy of the fluid particles can then be neglected; declaring the other terms of mechanical energy in the equation is much bigger. The linearized form of the equation becomes, (McCormick, 2010):

$$\boldsymbol{\eta} = -\frac{1}{g}\frac{\partial \phi}{\partial t}\Big|_{z=\eta} \tag{2.36}$$

2.3.2.4 Linearized free-surface boundary condition

The linearized free-surface condition is obtained by combining the dynamic and kinematic free surface boundary condition, at the vertical free-surface displacement.

$$\left\{\frac{1}{g}\frac{\partial^2 \phi}{\partial t^2} + \frac{\partial \phi}{\partial z}\right\}\Big|_{z=\eta \cong 0} = 0 \tag{2.37}$$

2.3.3 Boundary conditions for fluid and structure interactions

In order to fully describe the fluid domain the floating raft structure also needs to be regarded. Therefore applying the body and far field boundary condition completes the flow formulation.

2.3.3.1 Body boundary condition

Attention is now given to the flow of the vicinity of the rafts. The body condition declares that no flow can cross the surface boundary of the raft. This is achieved by stating the normal velocity of the fluid at the submerged body surface S_B is equal to the normal velocity of the floating body. This is expressed by:

$$\frac{\partial \phi}{\partial n} = \frac{\partial \boldsymbol{s}}{\partial t} \cdot \boldsymbol{n}\Big|_{S_b} \tag{2.38}$$

Where s is the displacement vector of a point **x**, each point of the wetted surface is described by **x**=S_b and **n** is the normal unit vector pointing outward of the surface. An excellent description of how to formulate the displacement vector **s** is found in Kraemer's report section 4.4.2 (Kraemer, 2001).

2.3.3.2 Far-field boundary condition

This condition states that the radiated waves from the body is fading further away from the body. By introducing the radial distance in x and y direction as $r = \sqrt{x^2 + y^2}$, this can be mathematically formulated in the following way,

$$lim_{r\to\infty}|\boldsymbol{U}| = 0 \tag{2.39}$$

Stating that at an infinite distance from the body, there exist no radiated waves.

2.4 Velocity potentials

Mentioned in Section 2.3.1, the resulting flow of simultaneously occurring wave phenomena can be described by summarising the generated flows of each phenomenon according to the super position principle. In linearized wave theory it is also stated that flow can be formulated by velocity potentials. In this section the different wave phenomena and the resulting velocity potentials are explained.

2.4.1 Incident waves

For an irrotational, incompressible flow McCormick declares two product solutions for the velocity potential to satisfy the continuity equation, namely the Laplace equation. The product solutions are given first for standing waves, with perfect reflection and of travelling waves that is considered in this thesis.

$$\phi_{incident\ waves} = \phi_0 = X(x)Z(z)T(t) \tag{2.40}$$

And the travelling wave solution,

$$\phi = X(x \pm ct)Z(z) \rightarrow introduce\ \xi = x - ct \rightarrow \phi = X(\xi)Z(z) \tag{2.41}$$

Where ξ refers to a horizontal coordinate, defined for right running waves. By introducing the product solution in the Laplace equation for a travelling wave, the following result is obtained. For convenience terms are separated in the later equation.

$$\nabla^2\phi = 0 \rightarrow \nabla^2\langle X(\xi)Z(z)\rangle = 0$$

$$\frac{1}{X}\frac{d^2X}{d\xi^2} = -\frac{1}{Z}\frac{d^2Z}{dz^2} = -k^2$$

k is in this equation a constant. The expression has now transformed to ordinary differential equation, which has following general solution:

$$X(\xi) = C_\xi\, sin(k\xi + \alpha)$$
$$Z(z) = C_z\, sin(kz + \beta)$$

where C_ξ, C_z, α and β are arbitrary constants. By applying the linearized boundary conditions described above, the velocity potential can be determined for a travelling wave. McCormick describes the steps in detail (McCormick, 2010). However, the seafloor condition results in setting β=kh and without losing generality, α can be given a value of zero due to x and ξ also being arbitrary.

If $\boldsymbol{C_\Phi = C_z C_\xi}$ is introduced, the velocity potential can be rewritten to,

$$\phi_0 = X(\xi)Z(z) = C_\phi \, cosh[k(z+h)] \, sin(k\xi) \tag{2.42}$$

This expression is substituted into the linearized dynamic boundary condition. The waves to be considered are sinusoidal in both space and time, why the following equality can be made.

$$\boldsymbol{\eta} = -\frac{\mathbf{1}}{g}\frac{\partial \phi}{\partial t}\Big|_{\boldsymbol{z=\eta}} = \frac{ckC_\Phi}{g}\cosh(kh)\cos(k\xi) = \frac{H}{2}\cos(k\xi)$$

From this the constant C_Φ can be determined and an expression for the velocity potential is derived. McCormick identifies *k* as the wave number and through next relationship additional parameters are introduced. These wave parameters are wave period *T*, wave frequency *f*, phase velocity *c* and the circular wave frequency *ω*.

$$kc = \frac{2\pi}{T} = 2\pi f = \omega \tag{2.43}$$

The circular wave frequency is used to reformulate the velocity potential. This is the equation for the velocity potential of incident waves, and is of great importance for this thesis.

$$\phi_0 = \frac{H}{2}\frac{g}{\omega}\frac{cosh[k(z+h)]}{cosh(kh)} sin(kx - \omega t) \tag{2.44}$$

Finally this expression is substituted in the linearized boundary condition, where McCormick obtains the formula for circular wave frequency.

$$\phi_0 = \frac{H}{2}\frac{g}{\omega}\frac{cosh[k(z+h)]}{cosh(kh)} sin(kx - \omega t) \rightarrow \left\{\frac{1}{g}\frac{\partial^2 \phi}{\partial t^2} + \frac{\partial \phi}{\partial z}\right\}\Big|_{\boldsymbol{z=\eta \cong 0}} = 0 \tag{2.45}$$

By simplifications and rearrangement of terms the following expression for the circular frequency is obtained as;

$$\omega = \sqrt{gk \, tanh(kh)} \tag{2.46}$$

2.4.2 Wave diffraction

The wave field will be changed by the presence of a floating body like the rafts. The wave diffraction or wave scattering, explained by Kraemer and Falnes, describes the effect due to the existence of a stationary body. The diffraction will cause forces on the rafts and is included in the wave excitation forces acting on the body. In linear wave theory this influence is formulated mathematically by the scattering problem and is solved by the diffraction velocity potential. A detailed derivation of the diffraction velocity potential and scattering force can be found in Kraemer and Falnes (Kraemer, 2001) (Falnes, 2002). Briefly the velocity potential for diffraction must fulfil the Laplace equation and satisfy given boundary conditions.

Attention is now given to the body boundary condition, stating that the normal velocity of the fluid at the submerged body surface S_B is equal to the normal velocity of the floating body. Because the rafts are restricted to move under the scattering problem, both the normal fluid velocity and the normal velocity of the floating body will be equal to zero.

The wave field is under these conditions fully described by the incident waves potential and diffraction velocity potential, as no radiation waves are generated due to the body is stationary. The body boundary condition will then become,

$$\frac{\partial \phi}{\partial n} = \frac{\partial \boldsymbol{s}}{\partial t} \cdot \boldsymbol{n}\Big|_{\boldsymbol{S_b}} = 0$$

No radiation gives

$$\frac{\partial \phi}{\partial n} = \frac{\partial [\phi_0 + \phi_{dif}]}{\partial n} = \frac{\partial \phi_0}{\partial n} + \frac{\partial \phi}{\partial n} = 0\Big|_{\boldsymbol{S_b}}$$

so,

$$\frac{\partial \phi_{dif}}{\partial n} = -\frac{\partial \phi_0}{\partial n}\Big|_{\boldsymbol{S_b}} \tag{2.47}$$

This implies at the surface of the body, diffraction causes a velocity of the fluid with a normal component that cancels the normal component of the fluid velocity due to the undisturbed incident waves. This can also be interpreted as no flow is going through the body.

2.4.3 Wave radiation

The alternation in the wave field due to an oscillating body in the absence of incident waves is described by wave radiation. The rafts here oscillate in otherwise still water, compared to diffraction where the body was held fixed in the presence of incident waves. The forces and momentums related to the radiation are called radiation forces and are included in the hydrodynamic coefficients. The hydrodynamic coefficients consist of added mass and wave damping coefficients, and are referring the oscillating body to act as a mechanical spring and damper system. It is well known that a body moving in water will generate waves, radiating concentric away from the body. Energy will be transported away from the body through surface waves. Analogous with a mechanical spring damper system, energy loss is related to the system damping. In wave theory the effect caused by radiated waves is therefore called radiation damping. The oscillating body will also be the source of water particles moving in phase with the rafts. According to Newton's law of motion a force greater than the particles inertia is required to achieve movement of the water particles. The added mass coefficient quantifies the portion of the waters inertia that has to be added to the inertia of the body to describe the mechanical system correctly.

The alternation in wave field due to radiation is formulated for every degree of freedom of the system and each velocity potential solves each degree of freedom individually. Hence, the radiation velocity potential is the summation of all velocity potentials solved for each degree of freedom. This can be done due to the principle of superposition.

$$\phi_{radiation} = \sum_{i=1}^{N} \phi_i \tag{2.48}$$

Where $\phi_{radiation}$ corresponds to the summerized velocity potential, ϕ_i is the velocity potential for each degree of freedom and N is the number of degrees of freedom.

A thorough explanation of the velocity potential, radiation force, added mass and radiation damping is given in Kraemer and Falnes, under similar boundary conditions that are applied here (Kraemer, 2001) (Falnes, 2002). Concisely the radiation velocity potentials must as all the other described potentials satisfy the Laplace equation. The body boundary condition, described in Subchapter 2.3.3.1, is once again to be investigated. The radiation problem is describing the oscillating body in the absence of incident waves. Diffraction is not considered here either, as the body is known to oscillate. At the rafts submerged surface, the normal velocity of the fluid is equal to the normal velocity of the floating body under the body boundary condition, which is now reduced to:

$$\frac{\partial \phi_{tot}}{\partial n} = \frac{\partial \phi_{radiation}}{\partial n} = \frac{\partial \boldsymbol{s}}{\partial t} \cdot \boldsymbol{n}\Big|_{S_b} \tag{2.49}$$

Where **s** is the displacement vector of a point *x*, each point of the wetted surface is described by **x**=S_b and **n** is the normal unit vector pointing outward of the surface. Mentioned earlier, the radiation velocity potential consists of all individual velocity potentials solved for each degree of freedom respectively. The freedom specific velocity potentials are also required to meet the body boundary condition, so

$$\frac{\partial \phi_i}{\partial n} = \frac{\partial s}{\partial t} \cdot \boldsymbol{n}\Big|_{S_b} \tag{2.50}$$

$$for\ i = 1, \dots, N$$

Where N equals the number of degrees of freedom for the system.

2.5 Hydrodynamic forces

Described in Kraemer, the response of floating bodies due to incident regular waves can be divided subsections, due to linearity. Here the different wave phenomena and wave potentials have been described in previous sections, and are now to be connected with the mechanical response of the floating body. Wave excitation force is the first sub problem, formulating the forces acting on a stationary body in presence of incident waves. An oscillating body concerning hydrodynamic loads related to the radiated waves causes the second sub problem with no incident waves present (Kraemer, 2001).

2.5.1 Wave excitation force

The wave excitation force consist of the forces and momentums due to undisturbed incident waves, also called the Froude-Krylov forces, and the diffraction or scattering forces due to a stationary body. The reason why the forces are summarized to one is because the forces are subject to the same boundary condition. In the wave diffraction section it was concluded that no radiation was present under the stationary body condition, which is why the radiation velocity potential can be neglected. The flow is described by:

$$\phi_{tot} = \phi_0 + \phi_{dif} \tag{2.51}$$

And the wave excitation force can be formulated as:

$$\boldsymbol{F_{wave\ exciation} = F_{Froude-Krylov} + F_{diffraction}} \tag{2.52}$$

The unsteady irrotational form of Bernoulli's equation gives the relation between the forces and the velocity potentials. In this case, zero gauge pressure is considered, giving,

$$\boldsymbol{\rho}\frac{\partial \phi}{\partial t} + \rho\frac{\boldsymbol{U^2}}{\boldsymbol{2}} + \boldsymbol{\rho} gz + p = f(t) = 0 \tag{2.53}$$

The linearized Bernoulli equation assumes that $\boldsymbol{U \cdot U}$ is of second order and can be neglected. The hydrodynamic pressure acting on the body is obtained first by stating that only dynamic pressure is considered. Secondly the total velocity potential is substituted by the potentials for diffraction and incident waves. The wave excitation forces can then be calculated by integrating the hydrodynamic pressure over the mean wetted surface S_b. A detailed derivation of this is to be found in Kraemer. Furthermore, Falnes presents the result of the wave excitation force only considering the spatial dependence by utilizing the frequency domain, executed to restrict the time dependence. The reader is recommended to acknowledge mentioned articles by Kraemer and Falnes regarding the details and explanation of the frequency methodology (Kraemer, 2001) (Falnes, 2002). The results presented in Falnes are given below.

$$\phi(\boldsymbol{x}; t) = Re\{\varphi(\boldsymbol{x})e^{-i\omega t}\} \tag{2.54}$$

$$\boldsymbol{F_{wave\ exciation}} = i\omega\rho \iint (\varphi_0 + \varphi_{diff}) n\, dS \tag{2.55}$$

$$\boldsymbol{F_{Froude-Kirloff}} = i\omega\rho \iint \varphi_0\, n\, dS \tag{2.56}$$

$$\boldsymbol{F_{diffraction}} = i\omega\rho \iint \varphi_{diff}\, n\, dS \tag{2.57}$$

2.5.2 Wave radiation forces

Radiation waves refer to waves generated from an oscillating body in the absence of incident waves, which are described in Section 2.4.3**.** By using the derived velocity potential, the hydrodynamic pressure in the i-th degree of freedom can be formulated with the linearized Bernoulli equation by Kraemer as

$$p_i = -\rho\frac{\partial \phi_i}{\partial t} \tag{2.58}$$

For a fully derivation of the following equations and the concept of phasor representation of time dependency, the interested reader is again encourage to look into the literature by Kraemer (Kraemer, 2001) and Falnes (Falnes, 2002). A short summary is given in order to enable an understanding of the formulas used to describe the forces acting on the rafts in the proceeding numerical simulations.

The time independent radiation force, evaluated for oscillations in the i-th degree of freedom, can according to Kraemer and Falnes be expressed in the frequency domain by the formulas given below.

$$\phi_{radiation} = \sum_{i=1}^{N} \phi_i \tag{2.59}$$

$$\phi(\boldsymbol{x}; t) = Re\{\varphi(\boldsymbol{x}) e^{-i\omega t}\} \tag{2.60}$$

Replacing the complex velocity potential in the linearized Bernoulli equation gives:

$$p_i = Re\{i\rho\omega\varphi_i e^{-i\omega t}\} \tag{2.61}$$

Integrating the hydrodynamic pressure over the mean wetted surface S_b, the complex radiation force in the frequency domain in the i-th degree of freedom becomes,

$$\boldsymbol{F_{radiation,i}} = i\omega\rho \iint \varphi_i \, n_{i'} \, dS \tag{2.62}$$

Where $n_{i'}$ represents the component of the outgoing normal unit vector in the i-th direction.

The oscillation of the semi-submerged body will transfer movement to the surrounding water, which in return causes the radiation forces acting on the body described above. Because the forces are described in each degree of freedom for the system, it can be convenient to express the radiation forces with Newton's second law of motion. This is conveyed in Section 2.6. The radiation forces will then be described by additional hydrodynamic coefficients, namely the added mass coefficient and radiation damping coefficient. The physical interpretation of the coefficients refers to the water movement occurring in presence of an oscillating body. Added mass refers to water particles moving in phase with the oscillations of the nearby body. Inertia is added to the system when these particles move with the body and the resulting force is the product of added mass coefficient times acceleration. The movement of water particles radiating away from the body is described by the radiation damping and can be seen as surface waves. The damping force is calculated as the velocity of the oscillating body times the coefficient of radiation damping. Kraemer describes this methodology by introducing a mechanical spring and damping system with one single degree of freedom (Kraemer, 2001). The mechanical system is illustrated in *Figure **9***.

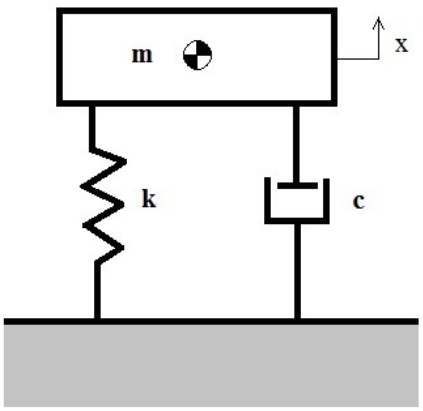

Figure 9 Mechanical spring and damping system

2.6 Motion of the wave energy dissipation device

Previous in this chapter the system geometry has been defined as well as the forces acting on the structure. A comparison was also given to a mechanical system with a single degree of freedom when formulating the added mass and radiation damping components of the radiation forces. This is shown in *Figure 9*. Newton's equation of motion wills for that mechanical system be formulated as:

$$(m + a)\ddot{x}(t) + (c + r)\dot{x}(t) + kx = f(t) \qquad (2.63)$$

Where *a* represent the added mass and *r* the radiation damping. The coefficients *m*, *c* and *k* represent the mass, damping coefficient and hydrostatic restoring force coefficient. In this case x represents the direction of the movement. The individual degree dependent coefficient will be gathered in matrixes when all degrees of freedom are to be considered simultaneously. The added mass coefficient will be gathered in the added mass matrix and the corresponding matrix for the radiation damping coefficient is called the radiation resistance matrix or added damping coefficient matrix (Falnes, 2002).

For this work, it is now possible to formulate the induced motion of the structure by the wave excitation force. In an analogy with the investigated system with semi-submerged oscillating bodies and connected dampers, Newton's second law of motion is formulated as the equation below. As each degree of freedom is considered, **x** is a matrix representing each direction of movement. The matrix formulation of the equation of motion for the investigated device becomes,

$$(\boldsymbol{M_s} + \boldsymbol{M_a})\ddot{\boldsymbol{x}} + \left(\boldsymbol{C_{damp}} + \boldsymbol{C_{rad}}\right)\dot{\boldsymbol{x}} + \boldsymbol{Kx} = \boldsymbol{F_{diffraction}} + \boldsymbol{F_{Froude-Krylov}} \qquad (2.64)$$

Where $\mathbf{M_s}$ represent the structural mass matrix and $\mathbf{M_a}$ is the added mass matrix. The damping term consists of the Radiation resistance matrix, $\mathbf{C_{rad}}$, and the damping matrix for the physical dampers, $\mathbf{C_{damp}}$, built in the device. **K** corresponds to the hydrostatic restoring force matrix. On the right hand side of the equation the external forces are summarised, which in this case exclusively is the wave excitation force. The wave excitation force acts on the structure by the diffraction force, $\mathbf{F_{diffraction}}$, and the Froude-Krylov force, $\mathbf{F_{Froude\text{-}Krylov}}$, which is induced by the incident waves.

3 Method

The performance of the suggested wave energy dissipation device is to be investigated. In order to evaluate a design at a stage before any physical models exist, the device is simulated numerically. How the wave characteristics influence the functionality of the structure is also to be examined. The purpose of this thesis is to determine the possibility to reduce wave energy in the spillway of a hydro power plant with the earlier described raft design. Therefore the performance of the device is evaluated in terms of energy dissipation efficiency. The parameters of the incoming waves that are to be considered are wave height, wavelength and wave period. In this chapter the assumptions of the investigation are stated and further explained. Attention will be given to the numerical software used, highly related to the theoretical background given previously.

3.1 Assumptions/ Preconditions

As previously mentioned the investigation is conceived in a manner so that a first scientific statement about the suitability to use the energy dissipation device for the suggested application is declared. In order to carry out the investigation within the limited time and computer resources, assumptions are needed to simplify the presented case. Besides the earlier mentioned aspects of economy and construction that not will be considered within this thesis, the investigation is also restricted to follow the limitations given below.

3.1.1 Wave considerations

The thesis will only consider regular waves hence the waves will have constant characteristics throughout each simulation. Changing one parameter of the wave will therefore result in another numerical simulation and thereby result in an additional data point. The waves are also stated to be linear, why Airy's wave theory is applicable. In order to treat the waves as linear, the wave steepness has to be low (McCormick, 2010). The wave steepness, also called the wave slope refers to the ratio of wave height divided by wavelength.

$$Wave\ slope = \frac{H}{\lambda} \tag{3.1}$$

Only waves with an incident angle of zero are considered. Consequently all the waves are assumed to hit the front face of the structure.

3.1.2 Deep water approximation

An important wave parameter to be considered simulating water waves is the distance between the still water line (SWL) and the seabed. The assumption relates the different wave characteristics to each other and the depth of the water will influence the formulation of this relationship. According to this theory, the flow conditions can be divided in three different categories; shallow water, intermediate water and deep water. For the deep-water approximation to be valid, the water depth should be at least half of the wavelength, $\frac{h}{\lambda} > 0.5$ (Sarpkaya & Isaacson, 1981).

According to Prof. Zhang this approximation is reasonable for the examined case (Zhang, 2014). The relation between the wavelength and wave period can according to the deep-water approximation be formulated as:

$$\lambda = \frac{gT^2}{2\pi} \tag{3.2}$$

Where g is the gravity acceleration coefficient, T is the wave period and λ the wavelength. This approximation also gives an expression of wave group velocity, c_g, as:

$$c_g = \frac{c}{2} \;\; and \;\; c = \frac{\lambda}{T} \tag{3.3}$$

Where c is called the wave velocity, defined as above.

3.2 Evaluation measure

In order to evaluate how much wave energy the device reduces, the energy dissipation efficiency is calculated. The approach taken in this thesis is to first calculate the power dissipated in the dampers - $P_{damping}$. Division with the energy flux of the waves obtains the dissipation efficiency in the dampers, referred to as $\eta_{damping}$.

$$\eta_{damping} = \frac{P_{damping}}{\dot{E}_{wave}} \tag{3.4}$$

The energy flux $\dot{E}_{wave}$ refers to the energy of the waves which path is occupied by the device. Because of the zero incident angle assumption, it is reasonable to presume that only the energy from these waves will excite the rafts. The energy flux will therefore be calculated for wave crest with equal width as the raft length. It is reminded the raft length refers to the y-dimension of the rafts, which are exaggerated in this investigation. By applying Airy's wave theory the equation for the wave energy flux for a given wave length (λ), raft width ($l_{y\,raft}$), the wave forward speed (c_g), the density of the water (ρ_{water}), the standard gravity (g) and the wave height (H) becomes:

$$\dot{E}_{wave} = Ec_g = \frac{l_{y\,raft} * c_g * \rho_{water} * g * H^2}{8} \tag{3.5}$$

The dissipation power of the dampers is related to the relative moment between the two structures. This case considers rotational dampers why the power is proportional to the relative angular velocity. The proportionality coefficient is the combined damping coefficient, b, and can be set by the simulation program. The unit for combined damping coefficient is [Ns/°] and the relative angular velocity $\dot{\theta}_{rel}$ has the unit [°/s].

$$P_{damping} = \left(b * \dot{\theta}_{rel}^2\right) \tag{3.6}$$

3.3 Computational tools

Numerical software utilized for the simulations are presented in this section, together with a concise description of the simulations procedure. A further explanation of the applied method of the simulations and the settings used are to be found in the continuing chapter. Special attention will also be given to the software AQUA LINE and AQUA NAUT and how they are connected.

Table 1 List of computational tools used in the thesis.

Step	Software	Usage
1.	DesignModeler, ANSYS Workbench	Define geometry
2.	Hydrodynamic diffraction (AQWA), ANSYS Workbench	Create mesh, define wave characteristics, connection between the rafts and fluid domain
3.	AQWA LINE	Hydrodynamic response in frequency domain
4.	AQWA NAUT	Motion response in time domain of the structures simulated. Angular velocity of the rafts exported and saved.
5.	MATLAB	Programming software, utilized to write files calculating e.g. energy dissipation efficiency. Used additionally to gather data and present result in graphs.

Briefly, the simulations procedure starts by creating a project in the software ANSYS Hydrodynamic diffraction (AQWA) part of the ANSYS Workbench configuration. Initially the geometry of the rafts is defined in the ad-in program DesignModeler. The mesh of this predetermined structure is then created in ANSYS Hydrodynamic diffraction. From the Workbench project, necessary parameters are exported and manually implemented in AQWA LINE in order to calculate the hydrodynamic forces in the frequency domain. In AQWA NAUT the time motion response of the structure in predefined waves is given. From AQWA NAUT the angular velocity of the two rafts can be found, which is used in MATLAB to calculate the dissipation efficiency. MATLAB is finally utilized in order to gather and present the results.

3.3.1 Calculation of Hydrodynamic forces in the frequency domain

The waves are considered to be harmonic and have small amplitude compared to their length, as discussed in the previous chapters. Further it is given that the fluid is incompressible and irrotational when using the potential flow theory as described under Subchapter 2.2.3. The 3-dimensional radiation/diffraction theory is used to compute the hydrodynamic fluid wave loading on floating rigid bodies.

The hydrodynamic forces are furthermore calculated alongside. These forces are a composition of radiation forces and fluid loading, as well as wave excitation forces and loading. The cause of radiation forces is described in detail under Subchapter 2.5.2. Briefly, these forces account the effect of a single body moving in still water.

The wave excitation forces and loadings, responsible for the body's movement, are calculated by summarising the diffraction force and Froude-Krylov force. The first one refers to scattering of the incident wave field and the second one refers to the pressure field in the undisturbed incident wave.

In order to develop the velocity potential within the fluid domain the Linear Superposition Theorem can be applied as the incident waves are of first order.

The hydrodynamic fluid forces are one part that is needed to depict complete calculation of the response of a floating body on the incident waves. Hence the second part is constituted of the hydrostatic fluid forces. Together with the body mass characteristics, AQWA LINE creates a so-called HYDRODYNAMIC DATA BASE. The database represents a full description of the hydrodynamic and hydrostatic conditions applying for each structure independently. The calculations performed by the software of the investigated bodies are carried out in the frequency domain. The created data base covers all calculated details of the fluid loading that are acting on the structure. The upper and lower limit of the database is set by the smallest and longest wave period. Evenly distributed intermediate values are thereafter calculated, in order to cover the entire area of investigation (Ansys Inc., 2009).

As the results are needed in time domain the hydrodynamic data base is processed further in AQWA NAUT to resolve the pursued data.

3.3.2 Calculation of the device's motion response in time domain

The numerical software AQWA NAUT is further used to simulate the floating rigid object as a motion response to regular linear waves. The hydrodynamic database created with AQWA LINE is taken to fully describe the movements of the rafts in the time domain at each time step for a certain period of time. Alongside goes the calculation of the instantaneous value of all other forces. Mathematical models (i.e. non-linear equations of motion) are used to derive acceleration of displacement of the applied structures (Ansys Inc., 2009).

3.4 Case definition

In this subchapter two investigation cases of the raft design are described in addition to the earlier mentioned wave parameters examined. This is combined with the implementation of numerical software, mathematical model and the related restrictions and limitations in succeeding sections. Thus the two different cases with three different variations each are presented here. Generalized descriptions are thereafter reinforced with actual data and settings. Consequently, an area of investigation is emerging from the practical implementations, examined parameters and chosen investigation cases. Related settings motivated throughout this chapter.

3.4.1 Investigation cases

As mentioned before two cases are investigated in more detail in this thesis. Each of the cases has three different variations, also called samples. In order to discuss the investigations in a scientific manner, the parameters of e.g. the incident waves or combined damping coefficient are always altered according to the same method. The simulation process and the settings are given after presenting the two different models and its variations.

In Section 2.1, the system geometry is illustrated. The raft width corresponds to the raft dimension in the wave direction (stated by the x-dimension in the coordinate system). The dimension in z-axis direction is referred to as the thickness, while the y-axis dimension is called the raft length. The first model depicted in *Figure 10* has constant dimensions with a raft length of two hundred meter in y-axis direction, a thickness of three meters in z-axis direction and a raft width of twenty meters in x-axis direction. Why these dimensions are set is further discussed later, motivating the selected starting point of the raft design. In the numerical simulation and the subsequent calculation of the dissipation efficiency a rotational linear damping system was assumed, which is a simplification of the model as it is intended in real use and pictured in the sketch.

The investigation case regarding the submerge volume of the rafts is called M6 and the result of this case are found in Subchapter 4.2. The sample variations of submerge volume are expressed by relating the rafts placement to the still water line (SWL). Thus the total area of submerged sidewalls is altered between 66%, 50% and 33%, which correspond to equal alternation of submerge volume. This procedure is carried out in order to examine if this influences the energy efficiency. By changing the weight of the raft, the submerge volume also changes according to the hydrostatic equation. This approach among others is used to change this parameter in the following simulations. The three samples are selected to give a wide range of simulations. The extreme cases are however not considered here, as it is reasoned the simulations and a real device would be more stable further away from these points. Due to time limitations, a more thorough investigation of the selected range or optimized level of submerged volume will not be included.

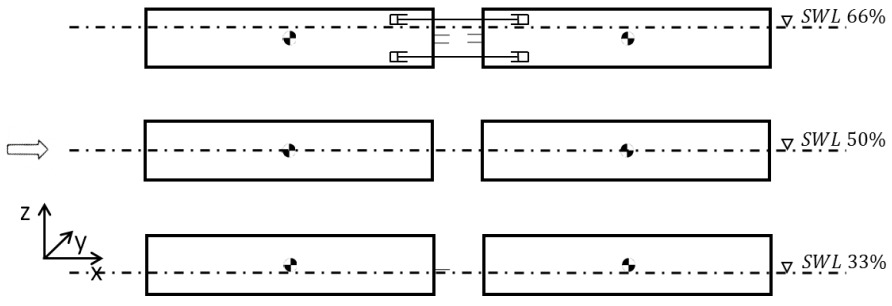

Figure 10 Model M6 and its variations investigated

How the energy efficiency is influenced by the raft width is to be observed by the second investigation case. In contrast to the first case, the second case pictured in *Figure 11* has no changes in submerged volume, keeping the volume constant at 50% within all three variations. F2 is the abbreviation used later in the report representing this model and its variations. Further constant dimensions are the raft length of two

hundred meter (in y-axis direction) and a thickness of one meter (in z-axis direction). In this case the width of the individual rafts is altering between twenty, fifteen and ten meters. Consequently the total volume of the device is also changing. The raft width alternations are thought to be covering a sufficient extent of the wavelength range in order to give a first statement of how this design parameter affects the energy efficiency.

Fifteen meters corresponds to the starting point of the design, described in section 3.5.1.1. Assuming that the density of the rafts is constant and the submerged volume is kept constant, the weight of the rafts changes with the alterations in dimensions. Corresponding values like the inertia of mass around the different axis is also alternated.

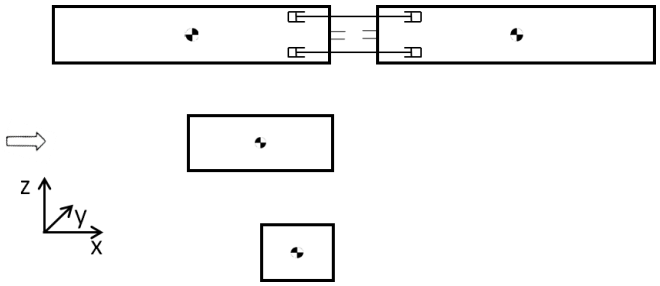

Figure 11 Model F2 and its variations investigated

3.5 Simulation procedure

In this subchapter the simulation procedure is presented. A flow chart is given in *Figure 12* in order to provide an overview of the different steps. The structure offered in the picture will be used throughout this subchapter, except the investigation cases that already has been presented. This section will answer questions about how the investigations will be simulated, how the setup is configured, what the cause is behind the settings and how the results will be derived.

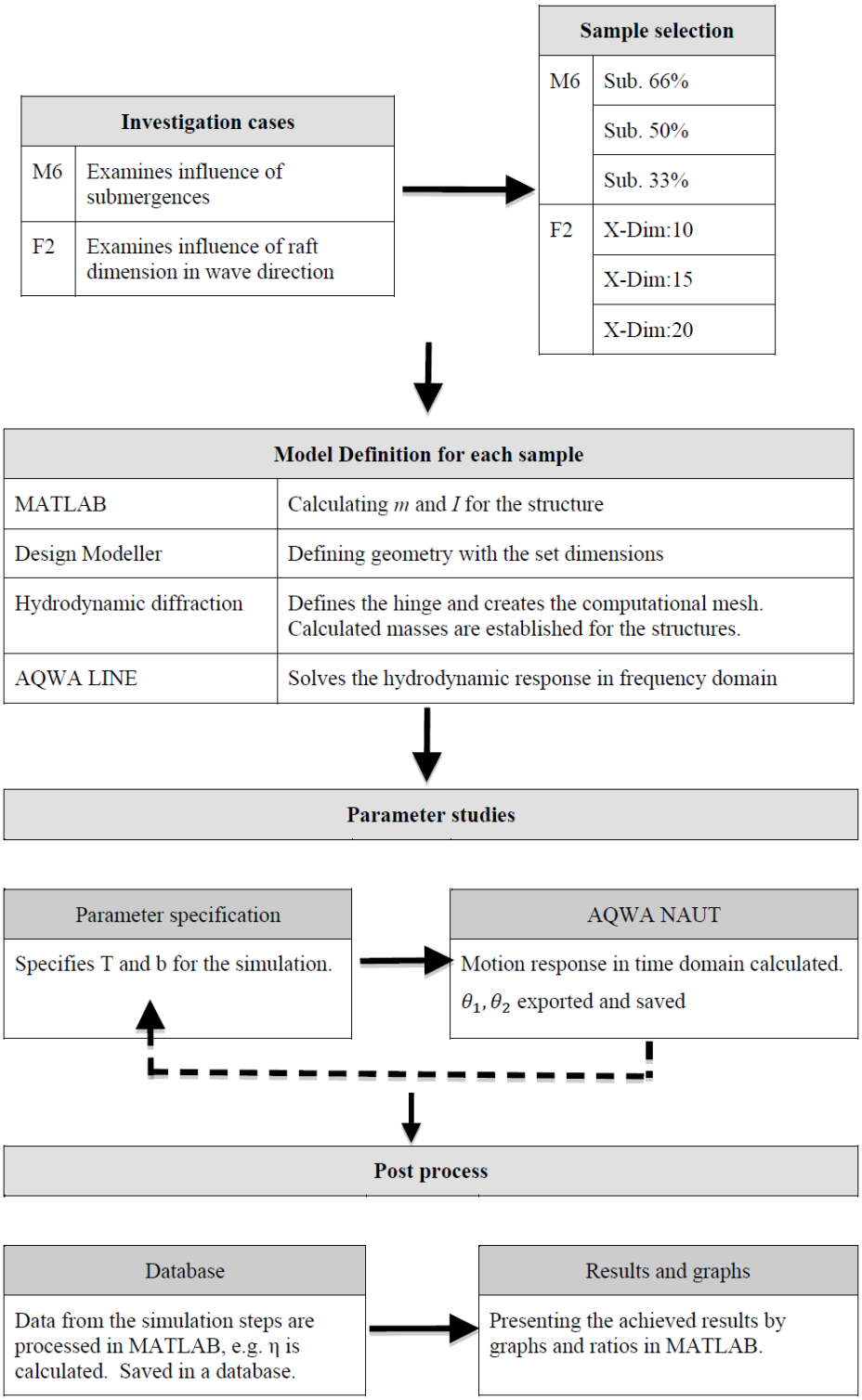

Figure 12 Flow chart of simulation procedure.

3.5.1 Model definition for each sample

The determination of two investigation cases and chosen variations of these are explained in detail in previous sections. This will result in a total of six different models, and are to be defined in this sub chapter. It is further described how these will be implemented in the numerical studies.

3.5.1.1 Starting point of raft dimensioning

According to Prof. Zhang, experience from previous investigations regarding the hydropower plant spillway shows that a wave spectrum of $T = 3 - 7\ s$ can be used as a default setting. The waves are also stated to have zero incident angles, reducing the effect of waves moving the structure sideways (Zhang, 2014).

A starting point for the design of the different cases was reasoned to be suitable for the investigation. By applying the deep-water approximation to the given wave spectra, a range of the wavelengths can also be calculated. In order to find a functioning structure for the entire range, waves in the middle of the spectra was considered to be dimensioning. A period of 5 s corresponds to a wavelength of 39 m. Literature and Prof. Zhang suggest that the highest energy dissipation efficiency is achieved when the raft is around $25 - 50\%$ of the wavelength (McCormick, 1987) (Zhang, 2014). With this result the starting point for raft width is determined to be around 15 m. How well this reasoning is investigated by the F2 case, resulting in three different models with variations in x-dimension.

The dimension in y-direction is set to have a considerable length in order to reduce the effect of waves breaking at the corners of the structure and to minimize possible effects of sideways motion of the device. Together with the restriction of zero incident angles waves, these settings are chosen so the two dimensional simplification is more applicable.

Described further in this section, a computational mesh is created in the software Hydrodynamic diffraction. Starting point for the raft thickness is set to be larger than the minimum cell size. The software limits the amount of cells leading to a specific lower limit of the cell sizes. In discussions with Prof. Zhang, it was decided that the thickness starting point should be around 1-3 m. M6 is determined to have a starting point of 3 m and F2 of 1 m.

3.5.1.2 Construction of the models

The starting point of the two different investigation cases has been established and the 3 variations for each case have been described. This will result in a total of 6 models required to perform numerical simulations with alternating parameters. The models are defined in the software DesignModeler where the dimensions are set. In the software the positioning of the rafts in reference to the SWL is predefined, which is utilized in the next step. With the dimensions set, complementing computations are made in MATLAB to calculate mass, centre of mass and inertia of mass around the different axis.

The surrounding environment of the device also needs to be simulated for each model, which is done in the Hydrodynamic diffraction-software. The standard settings for the fluid domain in the software are a water surface area of $1000\ x\ 1000\ \text{m}^2$ and the seabed is located at a depth of 1000 m.

These settings are chosen for all models, because the main prerequisite of applying the deep-water approximation is fulfilled. Because of the large structure, the computational mesh created in the same software will have the maximum amount of nodes allowed by the program in order to make the mesh as refined as possible. The size of the cells of the mesh will both influence the accuracy and the stability of the numerical simulations (Andersson, et al., 2012).

The damping unit connecting the two rafts is required to be defined for each model. Best suited to simulate the dampers was decided to be a hinge, where also the combined damping coefficient can be set. The hinge is arranged in a way so the relative motions between the two rafts are limited to rotation around the local y-axis, defined in the centre of the device. However, it is important to realize that the device is floating and can move freely in the fluid domain, whilst the connection determines how the rafts interact with each other.

None of the models are equipped with a mooring system, as the device is considered to be a free-floating object. This would be required for a real implementation of the device in a hydropower plant though the additional object would also influence the result. Hence the mooring system is left for further investigations. The simulations performed in this thesis will predictably ease the design specifications of that kind of system. A graphic view of a model created in the Hydrodynamic diffraction-software is found in *Figure 13*.

AQWA LINE is used to create a hydrodynamic database for each model. In the software 3-dimensional radiation/diffraction theory is applied to compute the hydrodynamic wave loading on the rafts, with the hydrodynamic forces calculated alongside in the frequency domain. This is explained in Section 3.3.1.

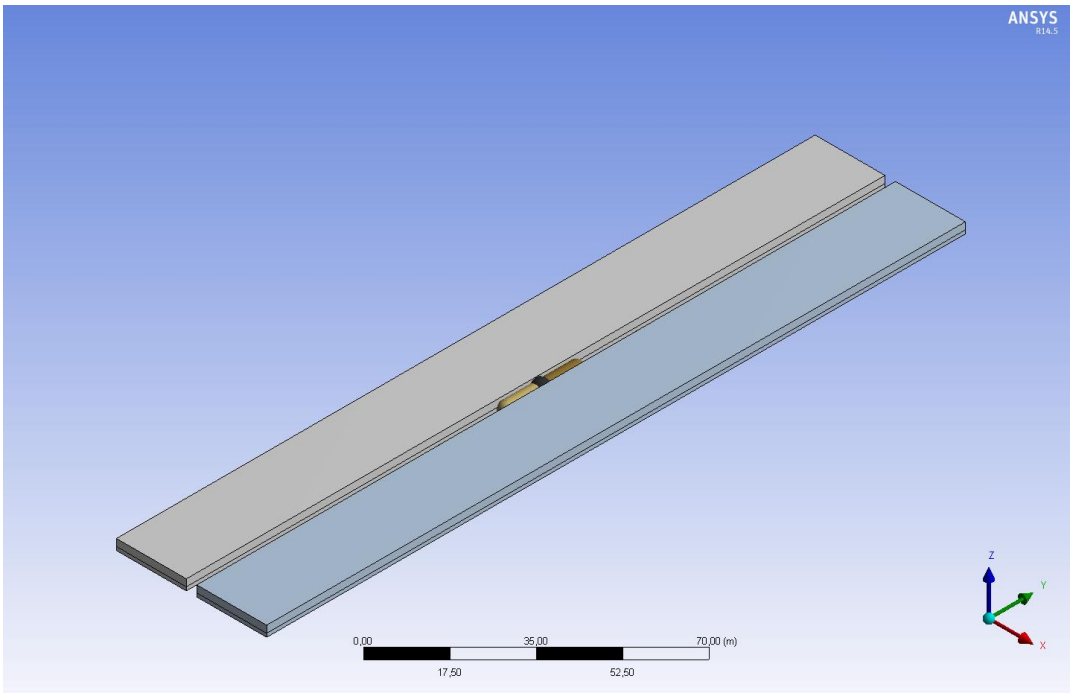

Figure 13 *Graphic view of model created in Hydrodynamic diffraction (ANSYS Workbench)*

3.5.2 Parameter studies

The numerical models created for each investigation sample are the foundation of the simulations performed with a set of alternating parameters. The simulations are conducted in the software AQWA NAUT. For every run the parameters need to be specified, which are held constant throughout the simulation. Results of each simulation will be exported and saved for post-processing. Then the procedure continues by changing one of the parameters again and a new simulation starts, and will be finished first when every possible combination of the alternating parameters has been simulated.

3.5.2.1 Parameter specification

A wave period spectrum of the investigation has already been established to $T = 3 - 7$ s, set after discussions with Prof. Zhang (Zhang, 2014). Data will be collected for each integer within this range, so there will be a reasonable amount of data points and satisfactory precision. This range will also directly correspond to a wavelength spectrum through the deep-water approximation, explicitly a range of $14 - 76.5$ m.

The second parameter to be examined is the combined damping coefficient (b), stating the resistance of the hinge-configured rotational damper in each model. By an empirical approach an area of investigation has been outlined. Through running several simulations with different models and settings, it was concluded a range of 10^4 -10^8 [Ns/°] would result in the highest energy dissipation efficiency, $\eta_{damping}$. Data was collected for each order of magnitude; explicitly b will alternate between 10^4, 10^5, 10^6, 10^7 and 10^8. Even if the peak efficiency will not be found with chosen settings, the empirical studies showed that the peaks would lie within the selected range.

In general, the time step in AQUA NAUT was set to 0.1 seconds and a finishing time of 100 s for the majority of the simulations. The calculations performed in the post-processing stage of the simulation procedure are time independent; however the time step was selected with the aim to give both stable and accurate solutions. There exist trade-of within numerical simulations, where small time steps can achieve high accuracy but also requires more resources and more computational time. Small time steps will additionally make the solution less stable (Andersson, et al., 2012). The finishing time were chosen so divergent result would be discovered, yet keep the computational time low. The wave amplitude was set to 0.5 m for all simulations.

3.5.2.2 Motivation of excluding wave amplitude variations

Mentioned earlier, pre-studies were performed before a system regarding the parameter specification was fixed that included the empirical studies of the combined damping coefficient. During this first stage of simulations, the wave amplitude was also alternating. Several of the suggested simulations could in addition not be performed, due to program limitations in AQWA NAUT. The program limitation state a wave slope steeper than 1/7 is not applicable for Airy's wave theory and sets the prerequisite of the settings. For the shortest wave period considered in this thesis, i.e. a wave period of 3 seconds, the amplitude is restricted to be below 1 meter. For the longest wave period, maximum allowed amplitude is around 5 meters.

Besides the program limitations, it was observed that the result from alternating the wave amplitude was very unpredictable, where small changes in amplitude or time period would have a huge impact on the energy efficiency. This was specially the case for waves with high amplitudes and a short period. Hence, supplementary simulations were performed with the aim to examine these deviations, where it was insinuated the result was less reliable when the wave slope was high. This can be seen in *Figure 14*, where the energy efficiency is plotted over the inverse wave slope. The dotted line perpendicular to the x-axis on the left hand side gives the limitation of AQUA NAUT and the right line represents the inverse wave slope of waves with a time period of 4 seconds and 1 meter in amplitude. The area between the two dotted lines represents simulations of waves with amplitudes of 1 meter and wave periods of 3 and 4 seconds.

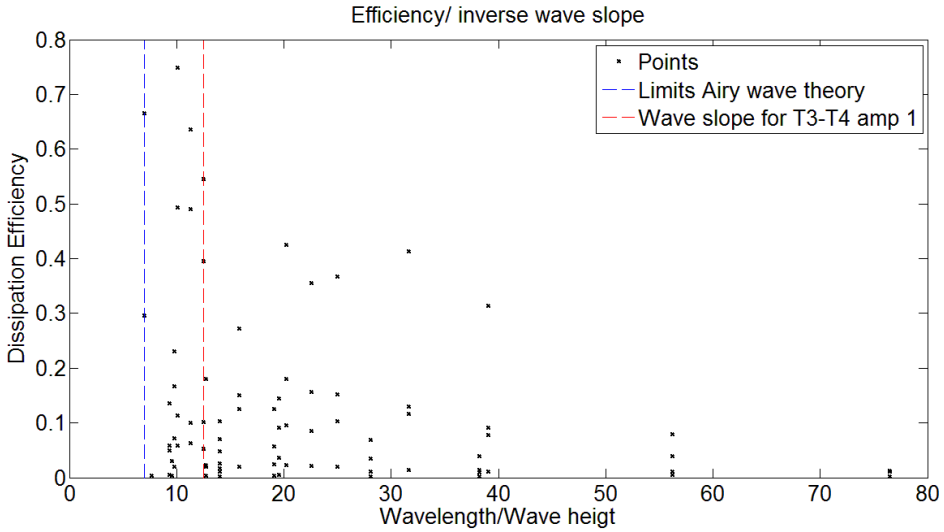

Figure 14 *Energy dissipation efficiency/ inverse wave slope, amplitude range of 0.5 - 5 m considered.*

Airy's wave theory is applicable when the wave slope is low (McCormick, 2010). This could be a reason why the result is highly fluctuating when the wave slope is approaching higher values. In *Figure 14* this is represented by values to the left as the inverse wave slope is depicted there. With this background, together with the fact only amplitudes below 1 meter can be simulated for the chosen wave spectrum, it was decided only waves with amplitude of 0.5 meters are to be simulated. The resulting plot of energy efficiency over inverse wave slope that is exclusively considering amplitudes of 0.5 m is presented in *Figure 15*.

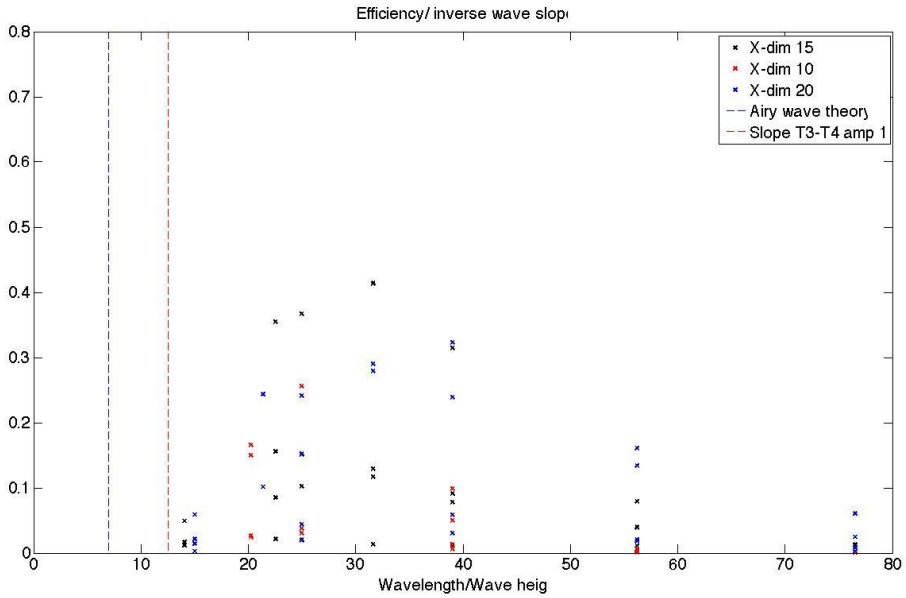

Figure 15 *Energy dissipation efficiency/ inverse wave slope, exclusively 0.5 m amplitude considered.*

3.5.2.3 Data-collection

In AQWA NAUT, the motion response of the structure with the set parameters is simulated in the time domain. In the program, a variety of factors related to the movement and forces of the rafts can be examined. In this thesis attention will be given to the dissipation efficiency of the device, which cannot be exported directly from the software. Instead the angular velocity around the y-axis is used as output and is later utilized in the post-process to calculate the factor of interest. The angular velocity is given for the two rafts independently for every time step. Just as important are the constant specified parameters described above which form the precondition for the motion response simulation. In addition, the energy dissipation efficiency is directly proportional to the combined damping coefficient and exponentially proportional to the wave height. For every simulation, the output from AQWA NAUT is saved together with the specified parameters and catalogued. The data is also distinguished from which model it is collected.

3.5.3 Post-process

Energy dissipation efficiency has been introduced as the evaluating measure for the investigations. First however the collected data needs to be managed into suitable forms. The output from previously step consists of the angular velocity for each raft in every time step. The energy efficiency is calculated from the relative angular velocity, which is the difference between the individual motion responses for each raft. Pursuing the steps described in Section 3.5, the energy dissipation efficiency can be calculated for each time step. This data is hence averaged in order to make the results more comparable and time independent.

After completing this procedure, a database is established where the energy efficiency result is saved together with the specified parameters and model classification. Each unique combination of parameter and model will correspond to one value of the dissipation efficiency. The database is arranged in matrix form, which can be structured accordingly to what parameter or model characteristic that is to be examined.

The data collection and the following database are compiled in the calculation software MATLAB. This software is also utilized in order to present the results in a comprehensible way, often in graphs that are seen in the next chapter. To indicate how different parameters influence energy dissipation efficiency, the large amount of data gathered is initially selected considering one varying parameter and the others held constant. The varying parameter and the resulting energy efficiency compose the axes of the majority of the graphs, from which the conclusion of the investigation will rely on. Each data point corresponds to one simulation in AQWA NAUT. Correspondingly, new choices of parameters with the respective data selections is used to create other graphs, where finally a wide selection of presented figures is established. The figures are thereafter compared with each other and as well put into context with findings in literature, in order to evaluate if the results are reasonable and confirm if tendencies can be indicated.

4 Results and discussion

Outcomes of the simulation procedure described in the previous chapter will be presented here with explanation of what the result indicate. The two investigation cases will be explained separately. Both cases will be compared in the succeeding chapter instead, where a more general discussion is held concerning e.g. optimization, implementation and hydropower plant considerations.

All samples are examined with the predetermined setting span. In regions of dissipation efficiency peaks or when other interesting features are occurring, the parameter is changed in a more punctilious level in addition to the frame setting methodology. In the simulation part of the project, it was also found that certain combinations of the different models and parameters could not be simulated, denoted by the project as the simulation gap. This will be shown in the graphs and discussed further in Subchapters 4.1.3 and 5.2.1.

4.1 Investigation of raft width, F2

Data from several simulations has been processed for the three different investigation samples, with a varying x-dimension. The samples are explicitly named after the width of one raft: 20 m, 15 m and 10 m. In this section, the graphs of the sample with a raft dimension of 15 meters are shown. A table is introduced, summarizing the highest efficiencies and applied settings for each sample. In the following subsections the result of wave period/wavelength will be discussed, comparing all the samples related to this investigation case. This will also be done for the combined damping coefficient.

The first graph presented is the energy dissipation efficiency plotted over combined damping coefficient for the sample with 15 m in x-dimension. The graph is shown in *Figure 16*, where the energy dissipation efficiency is dimensionless, wave period in [s] and the combined damping coefficient is given in [Ns/°]. For each line, the period is held constant and the connected data points correspond to that specified period and an alternating damping coefficient. The 5 lines in the figure cover the complete wave period spectrum. It is acknowledged that the highest efficiencies for this sample are achieved by a damping coefficient around 1 MNs/° for all wave periods, and peak efficiency of 36,7 % is discovered at the wave period of 4 s. In this report, 1 MNs/° is moreover referred to as 10^6 or 1e6 Ns/°.

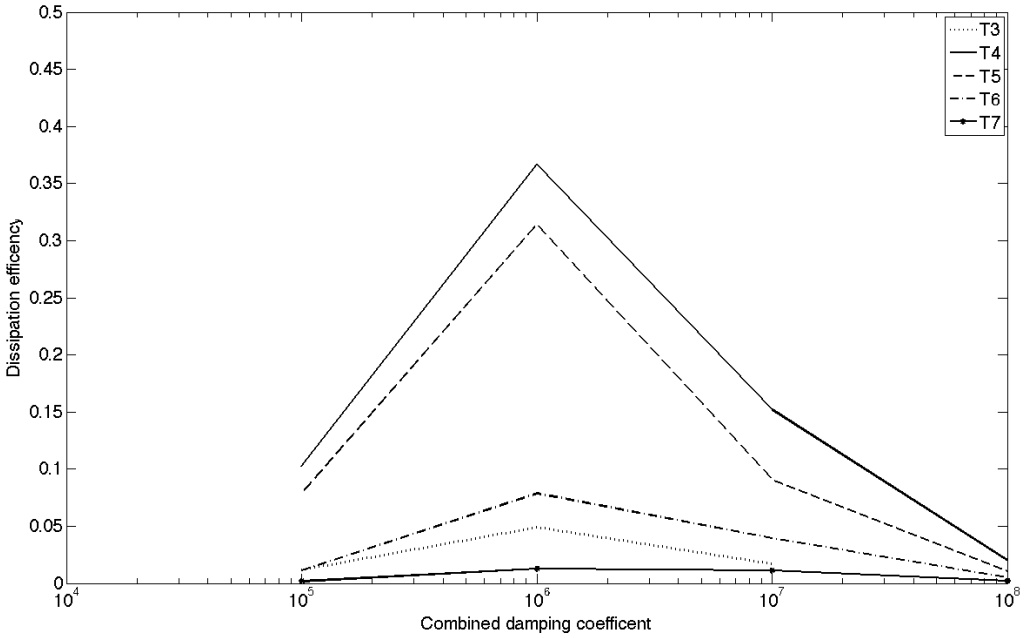

Figure 16 *The resulting dissipation efficiency of investigation sample X15 for alternating combined damping coefficient.*

Secondly the combined damping coefficient is held constant as the wave period is alternating for a sequence of simulations. This is presented in *Figure 17*. Following the different lines shows how the energy dissipation efficiency is varying with the wave period, and where each line is representing a single combined damping coefficient.

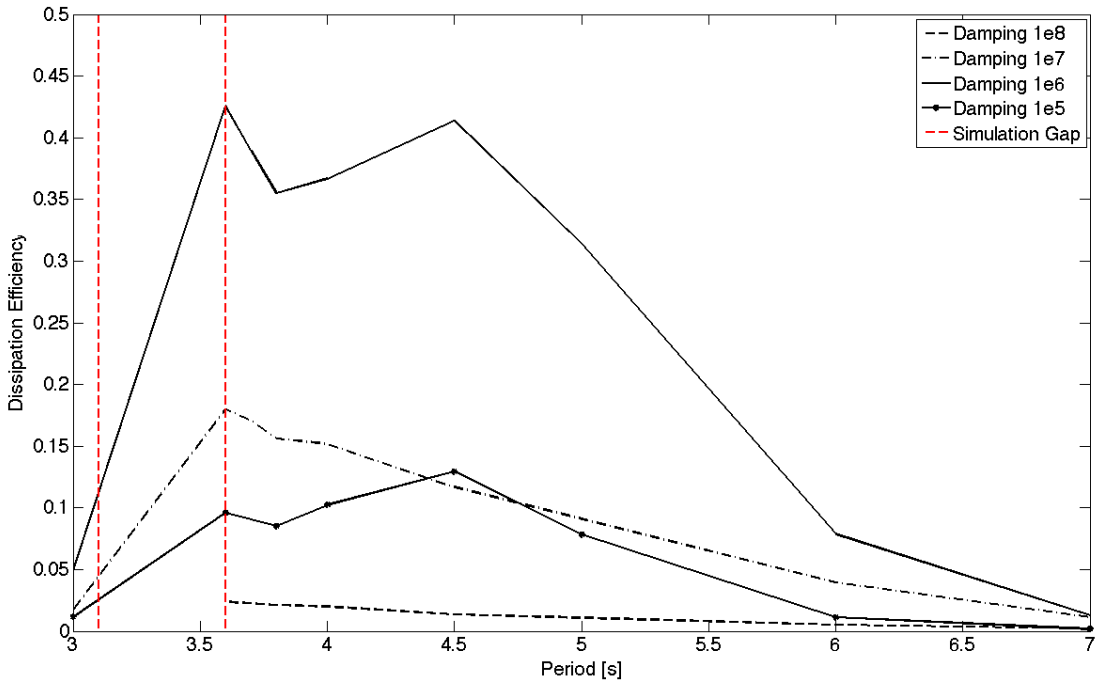

Figure 17 *The resulting dissipation efficiency of investigation sample X15 for alternating wave period.*

In the graph an area is marked with two vertical lines. This area expresses the simulation gap found for this investigation sample. Within this period range of 3.1-3.6 seconds, no converging solution exists, regardless of the combined damping coefficient used in the simulations. This phenomenon occurs also for the other two samples, though for different wave period ranges. Because no calculation of the dissipation efficiency can be performed within this area it is not possible to state any value of the efficiency. Hence linearizations were executed between the data points before and after the range, in order to complement the graph.

Figure 17 indicates an efficiency increase close to simulation gap. According to this observation, several simulations were performed to be able to examine the reliability of this result. Large variations in efficiency by small changes in wave period were discovered close to the simulation gap region. The accuracy and reliability of the result was questionable, both by the additional investigations as well as deviating result was salience in this nearby region. It was decided that a linearization should be performed in order exclude values in the direct region of the simulation gap. The sudden efficiency increase was thereby discounted. The graph presented in *Figure 17* is thus transformed into *Figure 18*, where a star represents the deviating result of the efficiency increase.

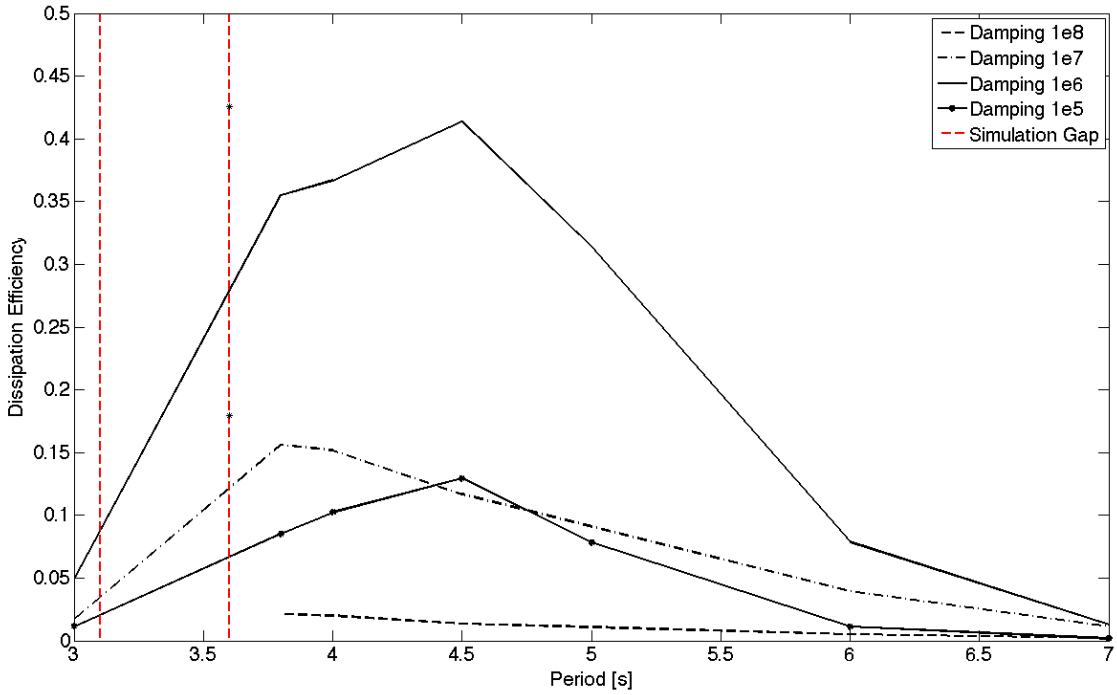

Figure 18 *The resulting dissipation efficiency of investigation sample X15 for alternating wave period. Deviating data points from the adjacent simulation gap region is excluded by linearization.*

It is acknowledged additional simulations have been performed for this sample besides the ones suggested according to the frame parameters. In order to give a more precise answer to where the efficiency peak occur and to validate the result, the wave period parameter is set with intermediate values of the predetermined integers for test check simulations.

This is why the simulation gap was not found in the previous figure where only the frame parameters of the wave period were considered. This is also the reason the peak efficiency is stated to be 41.4 % in *Figure 17*, for this investigated sample at a wave period of 4.5 s. This is in contradiction to *Figure 16*, stating the peak efficiency is 36.7 % at a period of 4 seconds.

Corresponding graphs for the other two samples are located in Appendix A. Short summaries of the peak efficiencies and simulation gap are given in *Table 1*, for every sample and the settings used to achieve them. Nonetheless the result for simulations with alternating wave period, wavelength and damping coefficients are compared and discussed in proceeding subchapters for all three investigation samples.

Table 2 *Summary of investigation case F2, examines the influence of X-dimension.*

Sample selection [m]		Maximum eff. [%]	Wave Per. [s]	Comb. Damping coef. [Ns/°]	Simulation gap
F2	X-Dim:10	25.6 %	4 s	1e6 Ns/°	T < 3.6 s
	X-Dim:15	41.4 %	4.5 s	1e6 Ns/°	T = 3.1-3.6 s
	X-Dim:20	32.3 %	5 s	1e6 Ns/°	T = 3.1- 3.4 s

4.1.1 Assessment of combined damping coefficient, F2

By composing a graph with a varying combined damping coefficient for all three different samples simultaneously, a discussion can be held for the investigation case in general and for the influence of combined damping coefficient in particular. This will be shown in *Figure 19*. Evaluation parameter is consistently the dissipation efficiency and the wave period is constant for all samples in order to reduce the number of alternating parameters and therewith the related result variations. In this assessment the wave period is selected to 4 seconds. This is because this wave period is part of predetermined frame parameter range and simulations have been completed for all F2 samples with high efficiencies as outcome.

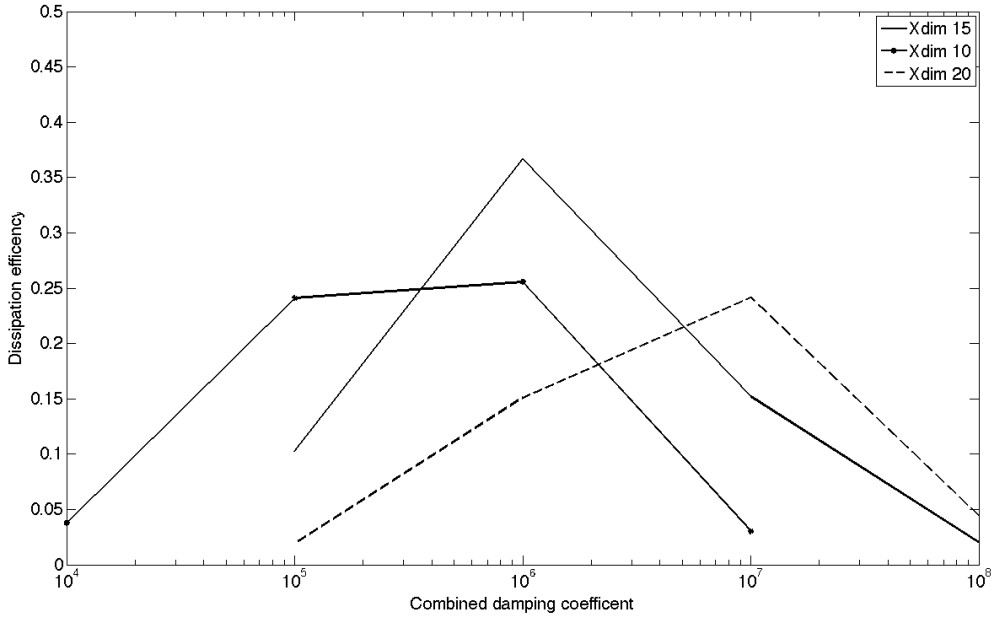

Figure 19 *Comparison of all the F2 samples for alternating combined damping coefficients. The resulting dissipation efficiencies are shown for a constant wave period of 4 seconds.*

In *Figure 19* it is shown that for a constant wave period of 4 seconds, the efficiency peaks of different samples are simulated within the chosen range of combined damping coefficient. Similar patterns of the dissipation efficiency over combined damping coefficient are also shown in *Figure 16* and Appendix A. This means the efficiency peak for approximately all wave periods included in the spectra is found within this range. In *Table 2* it is also acknowledged current settings are comparable to the settings used to achieve maximum efficiencies for the different samples. Hence it is concluded that the chosen range is suitable for the simulations conducted on behalf of this investigation case, despite only the result of one wave period is presented here.

Besides validating the selected range of combined damping, it is also shown that wider raft designs reaches peak efficiency at higher damping coefficient than compared to smaller designs. No optimization of the rafts will be conducted within this master thesis; however this will presumably be an important design consideration for further investigation.

4.1.2 Assessment of wave period and wavelength, F2

The wave period influence of the dissipation efficiency is furthermore investigated. According to *Table 1* the maximum efficiency for all samples is observed when the damping coefficient is set to 1e6 Ns/°. Logically, the same settings are therefore used when the different samples are compared regarding alternating wave periods. The composed graph is shown in *Figure 20*, where each line represents different samples with the same constant damping coefficient.

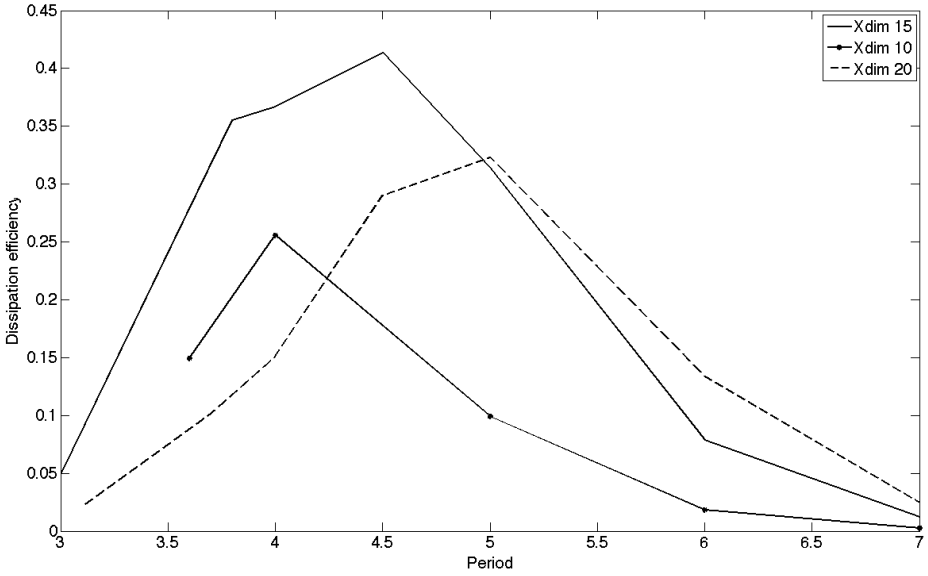

Figure 20 *All F2 samples compared for alternating wave periods. The resulting dissipation efficiencies are shown for a constant combined damping coefficient of 1e6 Ns/°.*

Figure 20 shows that the rafts with a constant combined damping coefficient of 1e6 Ns/°, all have peak efficiencies within the investigated wave spectrum, regardless of the sample simulated. For the sample with an x-dimension of 15 meters the efficiencies are lower at the outer points of the wave period range. This is true for all investigated combined damping coefficients and can be seen in *Figure 17*. The same outcome is also displayed in Appendix A, for the other two samples with x-dimensions of 10 respective 20 meters. This indicates the suggested raft design is well fitted for the investigated wave conditions that are assumed to apply. Referring back to *Figure 20*, it is also concluded that the highest efficiencies will occur at longer wave periods if the dissipation device is designed with wider rafts.

In order to be able to generalize the raft design for the applied wave conditions, a dimensionless number in the form of a ratio will be introduced. The advantage of using dimensionless numbers is the possibility to give a specific suggestion of raft design for the expected wave span applied. Stated earlier, the wave period will be directly proportional to a corresponding wavelength due to the deep-water approximation. A procedure of sorting the simulation result according to the total structure width in relation to the set wavelength has therefore been carried out. The total structure width of a two-raft dissipation device is calculated according to the formula below.

$$Total\ structure\ width = (2 * raft\ width) + distance\ between\ rafts.$$

Distance between the rafts constitutes the space where the hinge is to be fitted. For this investigation case it was chosen to 2 meters. *Figure 21* presents all the three different samples simultaneously. The graph is composed in the manner discussed in this and previous subchapters, although now with wavelength divided by total structure width.

Based on the same reasons as for the previous plot of the dissipation efficiency with alternating wave period, is only one combined damping coefficient presented with a constant value of 1e6 Ns/°.

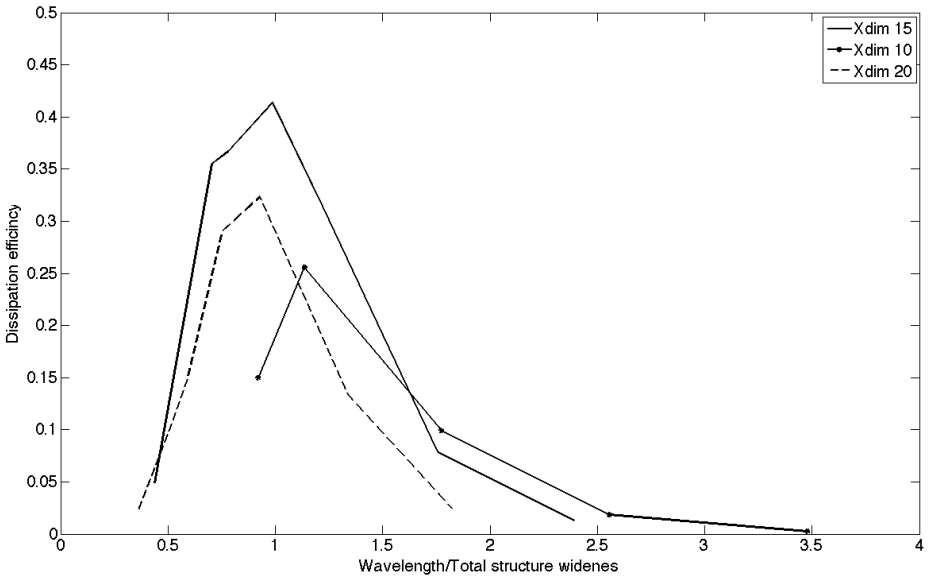

Figure 21 *All F2 samples compared for alternating ratio of wavelength per total structure width. The resulting dissipation efficiencies are shown for a constant combined damping coefficient of 1e6 Ns/°.*

Selected area of investigation for the F2 case has been validated in previous graphs, stating the chosen wave period spectrum and combined damping coefficient range is well matched. How the dissipation device should be designed is indicated from the result presented in *Figure 21*. The efficiencies are high when the ratio equals 1, when the total structure width corresponds to the wavelength. For instance one concept would be to match the raft design to the most frequently occurring wavelength. Why the sample with a x-dimension of 15 meters has the highest efficiencies in *Figure 21*, is most likely due to that the constant damping coefficient is best matched with this width. Variations in the combined damping coefficient are changing the order of which sample has the highest result; however the different samples are still having peak efficiencies around a ratio of 1. This is presented in Appendix A, in graphs composed for all samples and combined damping coefficient of 1e5 respective 1e7 Ns/°.

4.1.3 Assessment of simulation gap, F2

The simulation gap, listed in *Table 2*, was discovered rather late in the simulation procedure and found by coincidence. This was unexpected occurrence and will be discussed further in the general discussion. However, it is clear from the result in this investigation case that all samples have a simulation gap.

Simulation gaps are noticed for all examined damping coefficients and are located in the lower region of the wave spectra. It is also observed that wider raft designs have smaller simulation gap.

4.2 Investigation of raft submerged area, M6

A detailed description of how the presented data was treated in order to extract the relevant information of the M6 case is found in Subchapter 4.1. Hence the data extraction was carried out according to the investigation case F2, besides the linearization of results around the simulation gap. The methodology is consistent and the relevant results are discussed in this Subchapter. Data from several simulations has been processed for the three different investigation samples included in investigation case M6. The explicit denotations used here are 33%, 50% and 66% and represent the varying submerged area of both rafts. In these cases the raft dimensions are not changing as it was stated in subchapter 3.4.1. Main results, such as the highest efficiencies and applied settings for each sample, are presented in

*Table **3***. All relevant figures of sample 50% are discussed here and ought to be seen as descriptive examples. This is followed by graphs consisting of the significant data of all three sample variations. The focus is put on the potential relationship, similarities and differences. The individual graphs of sample 66% and 33% are located in the Appendix B.

In *Figure 22* the dissipation efficiency over the combined damping coefficient is plotted for the integer numbers of the wave period between 3 and 7 s. The complete wave period spectrum is covered in this graph. At a damping coefficient of 1MNs/° and a wave period of 5 s, an efficiency peak of 31.2% can be observed. It is recognized that the peak of the dissipation efficiency can vary between the combined damping coefficients among the different wave periods. Apart from a period of 5 s, the maxima are found at a combined damping coefficient of 1e7 Ns/°. Subsequently the focus will still be on 1e6 Ns/°, though the other samples also have the absolute efficiency peak at this combined damping coefficient. The results of these samples are presented in *Figure B.1* and *Figure B.3* in Appendix B. Thus an optimization towards an ideal combined damping coefficient is not obtained.

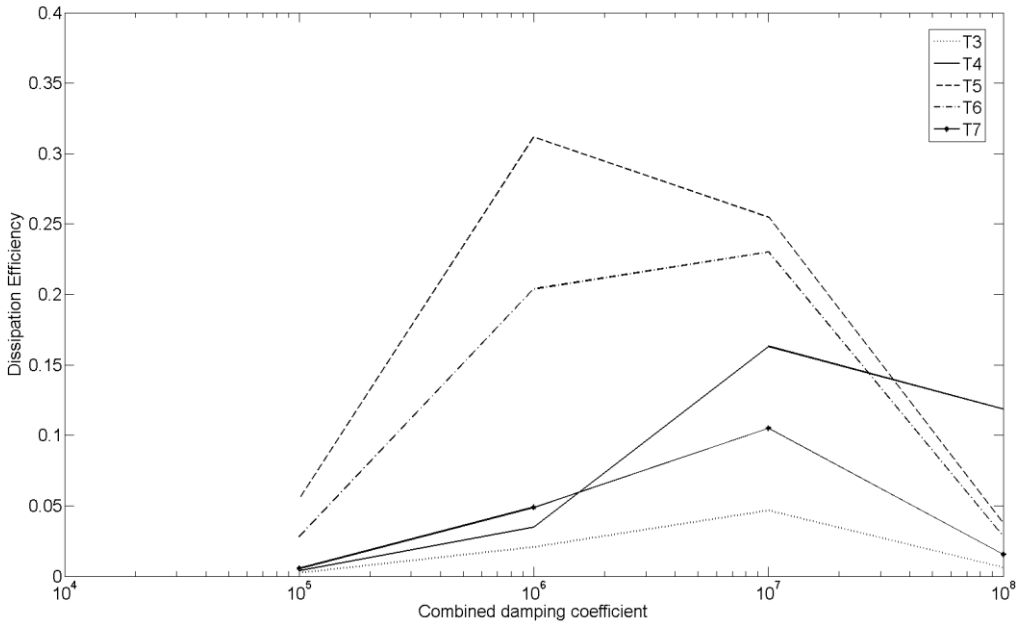

Figure 22 *The resulting dissipation efficiency of investigation sample 50% for alternating combined damping coefficient.*

Figure ***23*** represents the dissipation efficiency over the wave period for 50% submerged area for different combined damping coefficients. Within a period range of 4.1 to 4.5 s no converging solution of the simulation exists. This phenomenon occurs also for the other two samples, though for different wave period ranges.

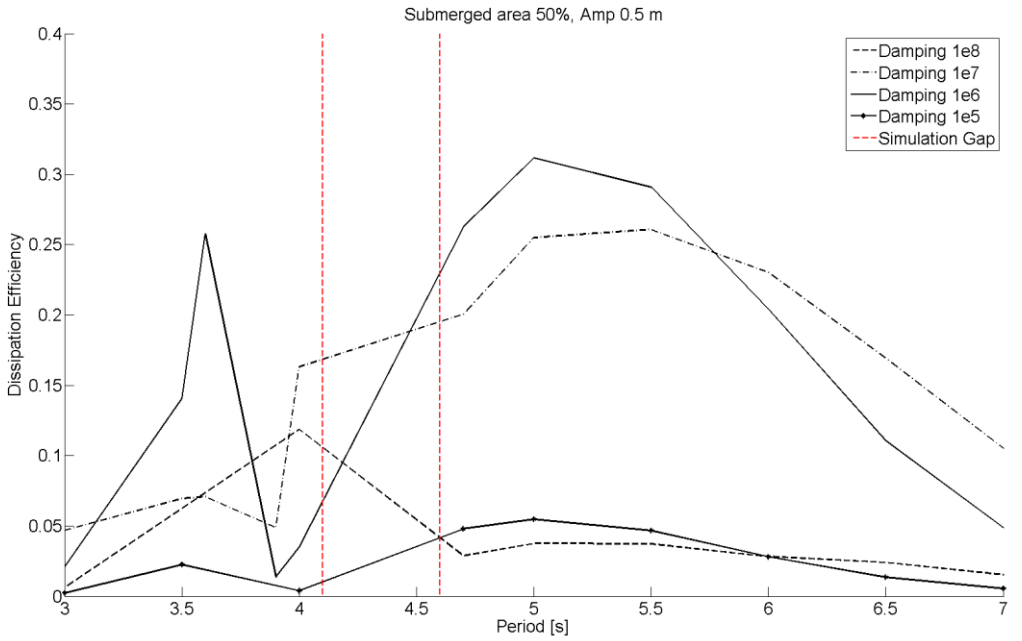

Figure 23 *The resulting dissipation efficiency of investigation sample 50% for alternating wave period.*

In *Table 3* a summary of the peak efficiencies and simulation gaps are given for every sample including the settings used. As for the F2 case, the simulation gap constantly occurs throughout a sample also when altering wave period or combined damping coefficient. The simulation gap width is smallest for a submerged area of 66% and largest for an area of 50%, but it cannot be reasoned to explain this change.

The maximum dissipation efficiency for 33% and 50% are at a wave period of 5 s, whereas for a submerged area of 66% the peak occurs at 5.5 s. Alternating the submerge area does not seem to change the value of maximum efficiency significantly, however it is indicated that the peak will occur at a different wave period. The amount of data is not sufficient to neither describe this relationship fully nor predict the behaviour of a real application. It is acknowledgeable however that the submerged area can be optimized for a specific wave period.

Table 3 Summary of investigation case M6, examines the influence of the submerged area

Sample selection [%]		Maximum eff. [%]	Wave Per. [s]	Comb. Damping coef. [Ns/°]	Simulation gap
M6	submerged: 33	30.43 %	5 s	1e6 Ns/°	T = 3.8 – 4.1 s
	submerged: 50	31.17 %	5 s	1e6 Ns/°	T = 4.1 – 4.6 s
	submerged: 66	33.31 %	5.5 s	1e6 Ns/°	T = 4.3 – 4.4 s

4.2.1 Assessment of raft submerged area to wave period, M6

In this subchapter the influence of the wave period on the dissipation efficiency is paired up with the results of all three samples and hence investigated. According to *Table 3*, the maximum dissipation efficiency for all samples can be observed at simulations with a specific damping coefficient set to 1e6 Ns/°. The corresponding settings are used when the results of the different numerical calculations are brought together in one graph as shown in *Figure 24*. Each line represents one sample for a constant combined damping coefficient calculated for alternating time periods. The method of linearization and removal of data points at the edge of the possible area of investigation has been followed for all three cases as well. Based on questionable results at a period of 3 s for 50% and 66% submerged area, they are excluded. In order to not withhold results the results including the questionable data points for each of the samples can be found under Appendix B.

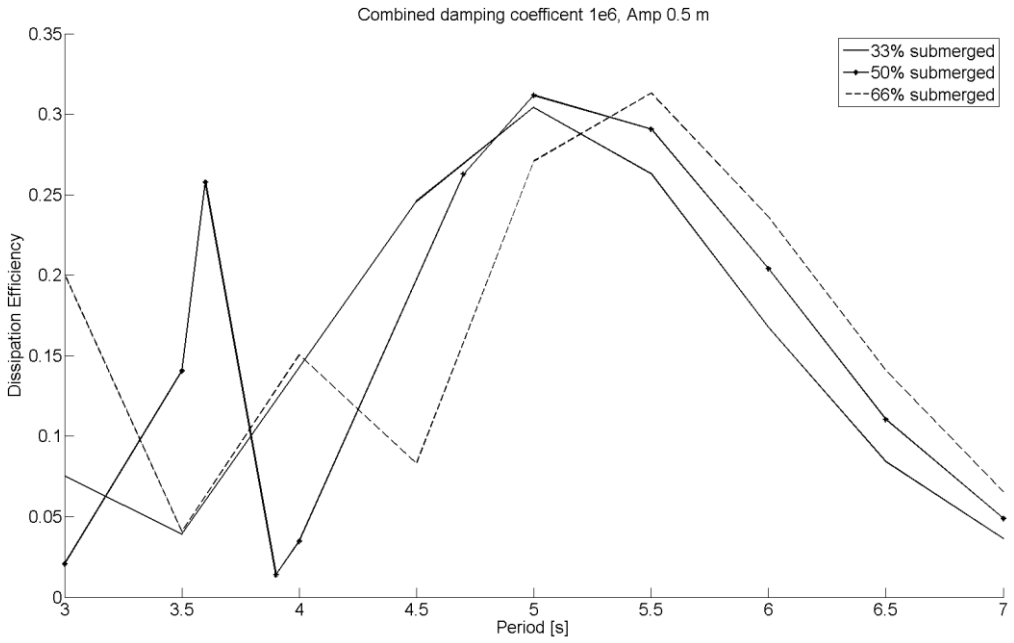

Figure 24 *Comparison of all the M6 samples for alternating period. The resulting dissipation efficiencies are shown for a constant combined damping coefficient of 1e6 Ns/°.*

Figure 24 shows the dissipation efficiency for the three samples for a constant combined damping coefficient of 1e6 Ns/° and alternating wave period. The peak efficiencies of the different samples are discovered within the investigated wave spectrum. Trends and patterns of all three samples are similar and not only is the peak efficiency within the same range of period between 5 and 5.5 s, it is also within the same figure of about 30%. As a result it can be stated that the investigated samples are very similar. Following the curve towards a higher or lower period the efficiency is decreasing significantly. All of these are indicators that the chosen raft design is well fitted for the investigated wave conditions that are assumed to apply. Hence it can be argued if the raft design should be optimized for a specific wave period in order to keep the wave energy dissipation device working at its highest efficiency. The benefits and the range are rather small which would make it difficult to communicate.

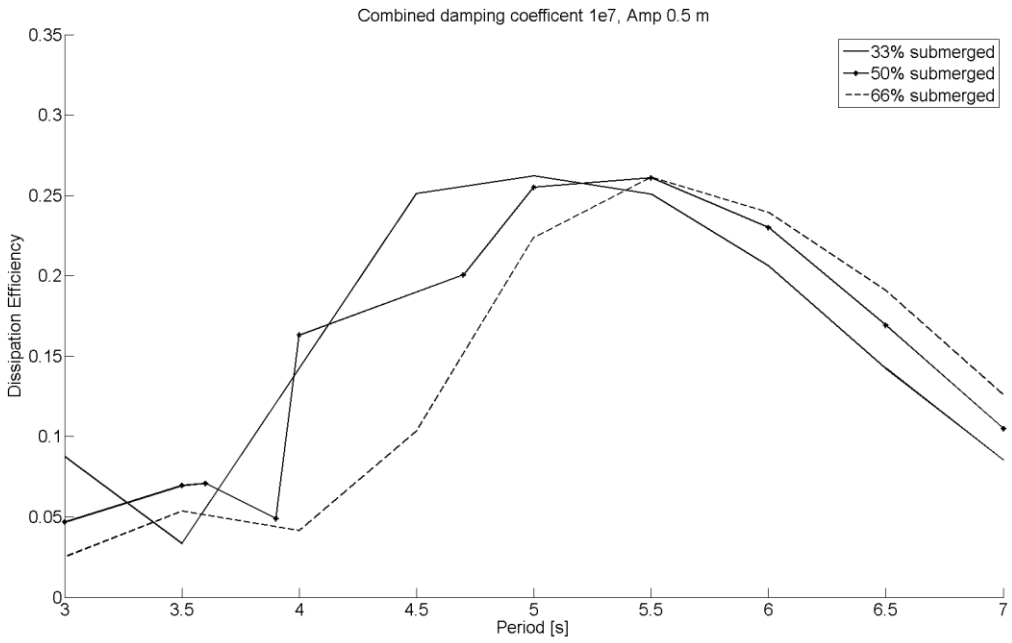

Figure 25 *Comparison of all the M6 samples for alternating period. The resulting dissipation efficiencies are shown for a constant combined damping coefficient of 1e7 Ns/°.*

Figure 25 shows the dissipation efficiency for the three samples for a constant combined damping coefficient of 1e7 Ns/° and an alternating period. Trends and patterns of all three samples are similar above a period of 5.5 s. The maximum dissipation efficiency is about 25% for all samples.

It is found that the suggested design with different submerged areas has sufficient designs. The best results can be found for the investigated damping coefficients of 1e6 Ns/° and 1e7 Ns/°. Changing the submerged area has only little influence on the dissipation efficiency. The patterns of the curves are similar in both cases and become more similar for periods above 5.5 s. These results are not able to validate the calculated set of data, but indicate a rather stable solution. In the following chapter the results discussed here are put in relation to investigation case F2.

5 General discussion

In this chapter the entire investigation of reducing wave energy in hydropower plant by the suggested wave energy dissipation device is discussed. First the result of both investigation cases will be summarized and discussed mutually on a detailed level and an effort given to validate the results. How the results are affected by the methodology and the simulation procedure in particular is also reviewed incorporating the choices of settings, assumptions, approximations and the software with its limitations. Special attention will be given to the simulation gap, discussion about underlying theoretical background to the simulations and the amplitude restriction.

The investigation is further put in a more general perspective, including a discussion about how the result can be interpreted and if the device would be applicable in a real case scenario. Improvements in form of design optimization and further recommendations are also included here.

5.1 Result interpretation

This thesis was carried out in order to be able to make a first scientific statement of the possibilities to utilize the suggested technology in a hydropower plant. The evaluation of the suggested technology was exclusively executed in the computational software, where several device designs was simulated and tested. The hydropower plant itself is not replicated, the simulation parameters are however set according to the wave conditions assumed to apply in the stilling basin of such a plant. The investigation is concentrated to the functionality and performance of the device and therefore only regards how efficiently incident wave energy is dissipated. No estimates of reduction in mechanical loads of stilling basin or local environmental issues e.g. erosion and sound pollution are presented in this report.

The simulations show peak efficiencies around 40%, which is satisfactory result and supports the idea of further investigations of suggested technology as a measure of decrease current problems related to high wave energy levels. Optimization of the design and simulation settings would probably improve the efficiencies greatly, giving even more promising prospect for this technology.

As no other investigations of this sort have been found, the results are hard to evaluate. If the objective shifts from the question if this technology is appropriate in a hydropower plant to just focus on the performance of the dissipation device, the results can be compared to results presented by Kraemer for simulations on McCabe Wave Pump. This device is also classified as a type of hinged barge system, though the design and application is different. The McCabe Wave Pump is developed to transform the incoming wave energy to useful piston work output, utilized to produce potable water and electricity. In the report by Kraemer, optimization of an existing prototype is conducted by analysing the model numerically. The investigated design consist of a three barge system, in combination of a submerge plate to stabilize the structure. The floating barges have two larger barges in the front and back of the system with equal length and the middle barge is smaller and connected to the submerge plate. From these design conditions it was also concluded that the highest efficiencies are expected to occur when the total structure width (by Kraemer referred to as total structure length) approximately correspond to the wavelength. This

supports the result obtained in investigation case F2 -clearly showing high efficiencies when the ratio of wavelength divided by total structure width equals 1.

Besides validating that the peak efficiencies occur with the similar set-up, Kraemer also present data about total power output over the incident wave power. The measurement presented there, as the total power output is the forces acting on the two dampers between the three rafts, which is utilized to run the earlier mentioned pistons of the MWP device. It is important to address that the simulations are not based on the same design, conducted in an identical manner or parameter selection. With this stated, the results of the two reports are still comparable and within the same order of magnitude. In the report written by Kraemer the optimization resulted in total power output increased from 34% to 87% of the total incident wave power input. The peak dissipation efficiency presented in this investigation is 41.4%, and occurs when the total structure width correspond to the total width. The dissipation device has though not been optimized, regarding e.g. combined damping coefficient. Notice the drastic improvement in efficiency accomplished by Kraemer by matching the design to the wavelength. Accordingly the design optimization resulted in an efficiency increase of 156 % compared to the original prototype, acknowledge by utilizing the resonance peaks within the system (Kraemer, 2001).

5.2 Discussion of the numerical simulations

The applied software, AQWA LINE and AQWA NAUT, was chosen in order to predicate the simulations on linear wave theory. Linear wave theory is greatly simplifying the fluid dynamic equations, and consequently the mathematical model of the forces acting on the structure generating the motion of the raft. How applicable the results are for a real case is difficult to predict. Several other methods of modelling fluid dynamics and fluid-structure interactions are available. Simulation of Floating wave energy converters in particular are discussed in the review article by Li and Yu. Mentioned simulation models include analytical methods, boundary integral equation methods and methods based on Navier–Stokes equation (Li & Yu, 2012). The method presented in this work is based on the linear wave theory, chosen on behalf of the limited time and computer resources available for this master thesis.

Stated in Section 3.1.1, the linear wave theory valid is for low wave slopes. Besides the limitations set by the program of a wave slope of 1/7, it was decided that only waves with amplitudes of 0.5 meter was to be part of the simulation result. The wave slope was hence restricted even more, in order to control the deviating data occurring close to this limit. How the amplitude influences the dissipation efficiency is yet to be examined, understandably the model created in this investigation is not suitable for this task. The reader is although reminded that the amplitude has already been investigated to a certain extent within this work. Mentioned in Subchapter 3.5.1, pre-studies were performed before a system regarding the parameter specification was fixed. During this first stage of simulations, the amplitude regarding the simulated waves was also alternating. It was observed the result from alternating wave amplitude was very unpredictable, where small changes in amplitude or time period would have a huge impact of the energy efficiency. Further examination showed that this in particular was true for wave simulations with high amplitudes and short wave periods, i.e. high wave periods. To reduce the impact of this phenomenon and the limitations described above, it was decided to exclude the entire wave amplitude alternation of the simulations.

Many simulations were however performed with higher wave amplitudes than the later fixed 0.5 meters, with still low wave slopes. These simulations with longer wave periods indicated no unpredictable behaviour, and were following the pattern observed in the fixed wave amplitude case. The efficiencies were generally smaller, approximately still within the same order. The lower efficiencies was also a reason why it was decided not to address this parameter in the report, even though a more thorough investigation has to be conducted before conclusions about the amplitude influence of dissipation efficiency can be drawn.

The relationship between the wave period and the wavelength was given by the deep-water approximation. For this approximation to be valid, the water depth should be at least half of the wavelength, $\frac{h}{\lambda} > 0.5$ (Sarpkaya & Isaacson, 1981). For the given wave period span the corresponding wavelength range reads $14 - 76$ m. For short wave periods, the deep-water approximation is acceptable for hydropower plants with a spillway deeper than 7 m onwards. In order for the approximation to be valid for the entire range, the water depth in the spill way should be at least 38 m. According to Prof. Zhang this is a reasonable approximation and more likely than the required condition for intermediate or shallow water approximation (Zhang, 2014).

5.2.1 Comments about simulation gap

The simulation gap was defined by the project as the combinations of different models and parameters, where no result could be simulated. The simulation gap was found for both investigation cases and for all samples within each case. It was indicated the wave period or corresponding wavelength was the decisive factor, as the simulation gap was given by a period spectrum and was there for the entire combined damping coefficient range tested. Generally the simulation gaps were located at the lower region of the wave period spectra and also deviating result was found in the nearby region of the gap.

It was shown that the simulation gap was wider for smaller rafts and at a lower period in investigation case F2. In the investigation of rafts submergences, M6, it also showed that the most submerged sample had the smallest simulation gap. Why this region of no converging solution alternates between the different samples needs to be investigated further. One theory is that the samples with a lower simulation gap are more stable, i.e. have less excessive movement, compared to the smaller and less submerged rafts. For the wider rafts the simulation gap occurs at longer wave periods.

Changing the focus from the appearance to the origin of the simulation gaps, a possible cause of this divergence might be the large size of the simulation model. The 3D model was designed to reduce the influence of wave forces in y-direction of the rafts and therefore the raft lengths were set to be very elongated. Both the size and the number of cells were set by program limitations of the computational mesh. A possible solution is to reduce the model size to create a more refined mesh. This is suggested as the coarse mesh might cause the gap, and the simulations are therefore expected to converge at these particular regions with finer cells.

5.3 Further investigations

Described previously in the result interpretation are the investigations presented within this master thesis, concerning the functionality and performance of the wave energy dissipation device. The purpose is to reduce local environmental problems and mechanical loads in the stilling basin. It is obvious that the relationship between the dissipated wave energy and reduction in mentioned concerns needs to be investigated further, among other things through empirical studies. Several critical points of real implementation of the prototype are additionally excluded in this thesis, such as cost considerations, manufacturing process or operating the device. Even though these aspects are of huge importance for implementing this kind of prototype, the further investigations suggested here will focus on further required analyses of the prototype before the implementation aspects are to be considered. In this section, suggestions for improving the simulation model are presented together with recommendations for design modifications. The prospect is to enhance the performance and suitability of the prototype by adapting it to the conditions applied in the hydropower plant.

In order to make the simulations more realistic, the investigation area needs to be broader. The conditions valid in hydropower plants ought to be examined closer, by data gathering and analyses. A more chaotic generation of waves are expected to apply in the stilling basin, why the wave settings in additional simulations ought not to be limited to linear regular waves with zero angle of incident. A different simulation method is also desired to utilize, that is unlike Airy's wave theory not restricted by the wave slope. The influence of wave amplitude of dissipation efficiency can hence be investigated.

A proposal to develop the model is to include a mooring system, which is identified as a prerequisite for a functional wave energy dissipation device. The influence of such a restoring force on the structure is necessary to evaluate. Several mooring systems have been discussed within this project, for example a basic concept with an elastic attachment with two-point connection between the structure and the stilling basin. It is also recommended to investigate multiple rafts, as more hinges presumably could increase the energy dissipation efficiency. It is indicated that the total length of the structure ought to be the length of the most frequently occurring wavelength, yet is this to be evaluated through supplementary simulations. An optimal design through simulations needs to be established by evaluating the suggested modifications and optimize the rafts dimension and combined damping coefficient, before proceeding empirical studies on real prototypes. The conditions valid in hydropower plants ought to be examined closer, by data gathering and further analyses to improve the simulation settings.

In summary, it is recommended to improve the presented model by introducing mooring system and additional rafts. The simulation settings should be changed to better correspond to valid hydropower plant conditions. Completing simulations by other methods and procedures are preferred, i.e. to investigate the wave amplitude.

6 Conclusion

The purpose of this thesis was to investigate how the energy dissipation efficiency of a given wave energy dissipation device is affected by a variety of incoming incident waves. This report has been the first scientific statement of the possibilities to utilize the suggested technology in a hydropower plant. It was accomplished by creating basic numerical models and conduct parameter studies on these. The parameter study was achieved by running several simulations with different settings in order to analyze incident wave conditions and damping modifications of the device. All simulations were according to Airy's wave theory. The dimensioning of the device has been investigated by two different cases; F2 investigated the raft width and M6 how submerge the device ought to be. F2 and M6, with three different samples each show peak efficiencies around 40% and 30% respectively. These results were satisfactory and support the idea of further investigations of suggested technology as a measure of decrease current problems related to high wave energy levels.

From the results of the F2 model it was concluded that the efficiencies were high when the total structure width corresponds to the wavelength. Such a clear relationship could not be found for the M6 case when changing the submerged area. It was found that the submerged area can be considered as a design factor, but the influence is not as strong as for the total structure width

The rudimentary of the models and the discussed limitations of the numerical simulations, caused a not neglectable amount of uncertainties and questionable results. One of them was the simulation gap, which was found in all cases and was wider for smaller rafts and at a lower period in investigation case F2. The investigation of the submerged area of the rafts in M6 gave very small variation in results. Thus it might be beneficial to consider when the floating energy dissipation device is optimized. In the M6 cases the simulation gap also occurred. Reasons for why region of no converging solution alternates between the different samples needs to be investigated further. One theory is that the samples with a lower simulation gap are more stable. Especially towards the limitations of the numerical model the results became questionable. In order to improve the results of the simulation the investigation area needs to be broader in the means of using valid conditions in hydro power plants, such as e.g. irregular wave theory and more advanced relation between the wave period and wavelength than the deep water approximation. The design of the raft should also be modified, by introducing a mooring system and additional rafts to potentially increase the dissipation efficiency.

Optimization of the designs and simulation settings would probably improve the efficiencies greatly, giving even more promising prospect for this technology. In order to improve the concept and validate the calculated result, it is suggested to build a physical model.

7 References

Andersson, B., Andersson, R., Håkansson, L., Mortensen, M., Sudizo, R., & van Wachem, B. (2012). *Computational Fluid Dynamics for Engineers.* The Edinburgh Building, Cambridge CB2 8RU, UK: Cambridge University Press.

Ansys Inc. (2009, April). AQWA™-LINE MANUAL - Release 12.0. United Kingdom.

Ansys Inc. (2009, April). AQWA™-NAUT MANUAL - Release 12.0. United Kingdom.

Cockerell. (1978). Apparatus for extracting enegery from wave movement at the sea. U.S Patent No. 4098084. Retrieved February 25, 2014

Encyclopædia Britannica. (2014, March 2nd). *Harbours and sea works 2014*. Retrieved from Encyclopædia Britannica Online: http://www.britannica.com/EBchecked/topic/254888/harbour

Falnes, J. (2002). *Ocean Waves and oscillating systems.* Cambridge, UK: Cambridge University Press.

Hagen. (1976). Wave driven generator. U.S. Patent No. 4077213. Retrieved February 25, 2014

Hales, Z. L. (1981). *Floating Breakwater: State-of-the-Art, Literature Pre- view.* CE, Fort Belvoir, Va.: U.S. Army Coastal Engineering Research Center.

Han, C., Zhao, J., Dang, Y., & Sun, F. (2009). Hydraulic Control of Safe Operation of large-scaled Hypervelocity Discharge Tunnel. In *Advances in Water Resources & Hydraulic Engineering* (p. 2284). Beijing, China: Springer Jointly published with Tsinghua University Press.

Hu, Z., Tan, X., & Xu, Z. (2014). China's Economy and Electricity Demand Outlook for 2050. In Z. Hu, X. Tan, & Z. Xu, *An Exploration Into China's Economic Development and Electricity Demand by the Year 2050* (pp. 161-178). Oxford: Elsevier.

IHA. (2000). *Hydropower and the World's Energy Future - The role of hydropower in bringing clean, renewable, energy to the world.* Compton, West Sussex, United Kingdom: International Hydropower Association.

Kraemer, D. R. (2001). *The motions of hinged-barged systems in regular seas.* Ann Arbor, MI, U.S.A.: Bell & Howell Information and Learning Company.

Li, Y., & Yu, Y.-H. (2012). A synthesis of numerical methods for modeling wave energy converter-point absorbers. *Renewable and Sustainable Energy Reviews 16*, 4352-4364.

McCabe, P. (1991). Wave powered mover. U.S. Patent No. 5132550. Retrieved February 25, 2014

McCartney, B. (1985). Floating breakwater design. *Wtrway., Port, Coast. andOc. Engrg., ASCE, 111(WW2)*, 304-318.

McCormick, M. E. (1987). A normal-mode analysis of the critically damped motions of hinged barges in regular long-crested waves. *Journal of Ship Research, Vol. 31(2)*, 91-100.

McCormick, M. E. (2010). *Ocean Engineering Mechanics - with applications.* New York City, U.S.A: Cambridge University Press,

copyright granted on 2014-08-26.

NDRC. (2013). *China's Policies and Actions for Addressing Climate Change (2013).* Beijing, China: The National Development and Reform Commission.

Novak, P., Moffat, A., Nalluri, C., & Narayanan, R. (2007). *Hydraulic Structures - Fourth Edition.* New York City, U.S.A.: Taylor & Francis, p. 245, Fig. 5.1,

copyright granted on 2014-09-16.

Persson, M. (2014, 03 18). Föreläsning 5/10 - Hydrodynamik. Gothenburg.

Roberson, J. A., Cassidy, J. J., & Chaudhry, M. H. (1998). *Hydraulic Engineering.* New York City, U.S.A.: John Wiley & Sons, Inc.

Sarpkaya, T., & Isaacson, M. (1981). *Mechanics of wave forces on offshore structure.* New York, USA: Van Sostrand Reinhold.

SCIO. (2012). *China's Energy Policy 2012.* Beijing, China: The People's Republic of China.

Stocker, T., Qin, D., Plattner , G.-K., Tignor, M., Allen, S., Boschung, J., . . . Midgley, P. (2013). *Climate Change 2013 The Physical Science Basis.* Intergovernmental Panel on Climate Change 2013. New York City, U.S.A.: Cambridge University Press.

Toy, T. J., Foster, G. R., & Renard, K. G. (2002). *Soil erosion: processes, predictions, measurement and control.* New York, U.S.A: John Wiley & Sons, Inc.

Verbund AG. (2007). *The power plants on the Austrian Drau.* Vienna, Austria: Verbund-Austrian Hydro Power AG,

copyright granted on 2014-08-20.

Zhang, Y. (2014). Professor at the Department of Hydraulical Engineering. *Personal and Electronic Communication 2014 January to June*. Beijing, China.

8 Appendix A

The graphs found in this appendix gather the simulation results of a sample included in investigation case F2. The sample presented here has a raft dimension of 10 m. *Figure A.1* and *Figure A.2* show the dissipation efficiency over combined damping coefficient and efficiency over wave period respectively. In the figures the energy dissipation efficiency is dimensionless, wave period in [s] and the combined damping coefficient is given in [Ns/°]. Peak efficiency of 25.6 % is found at a wave period of 4 seconds and a damping coefficient of 1 MNs/°.

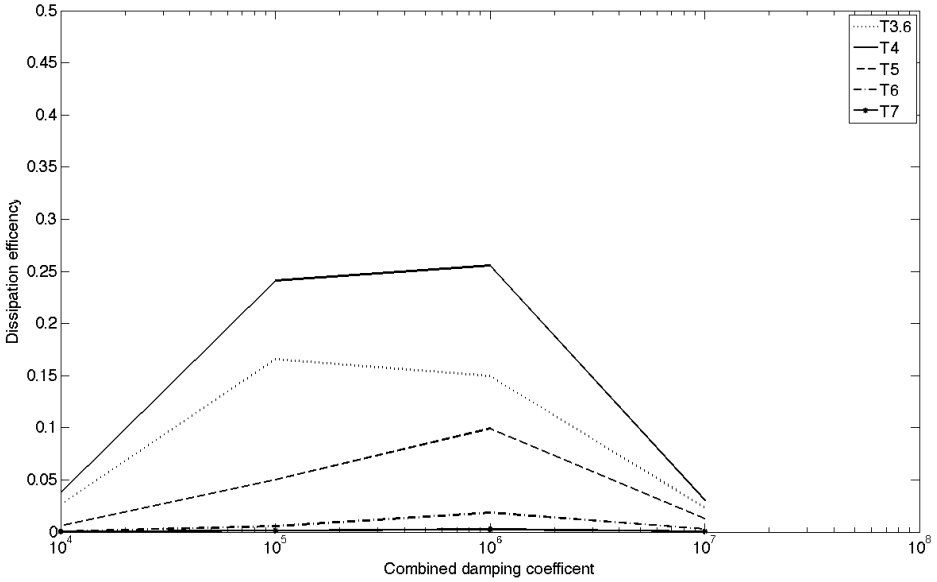

Figure A.1 *The resulting dissipation efficiency of investigation sample X10 for alternating combined damping coefficient.*

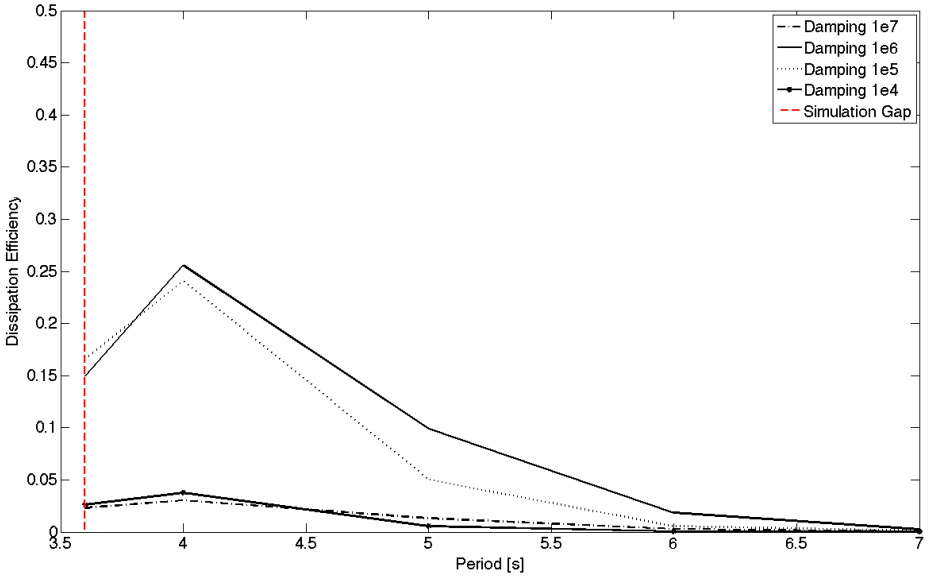

Figure A.2 *The resulting dissipation efficiency of investigation sample X10 for alternating wave period.*

The sample presented here has a raft dimension of 20 m. *Figure A.3* and *Figure A.4* show the dissipation efficiency over combined damping coefficient and efficiency over wave period respectively. Peak efficiency of 32.3 % is found at a wave period of 5 seconds and a damping coefficient of 1 MNs/°.

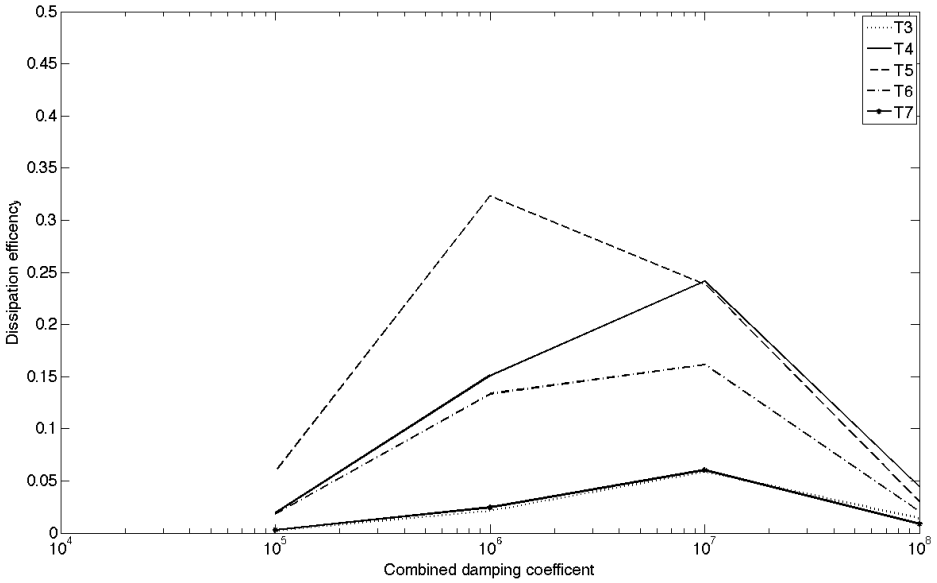

Figure A.3 *The resulting dissipation efficiency of investigation sample X20 for alternating combined damping coefficient.*

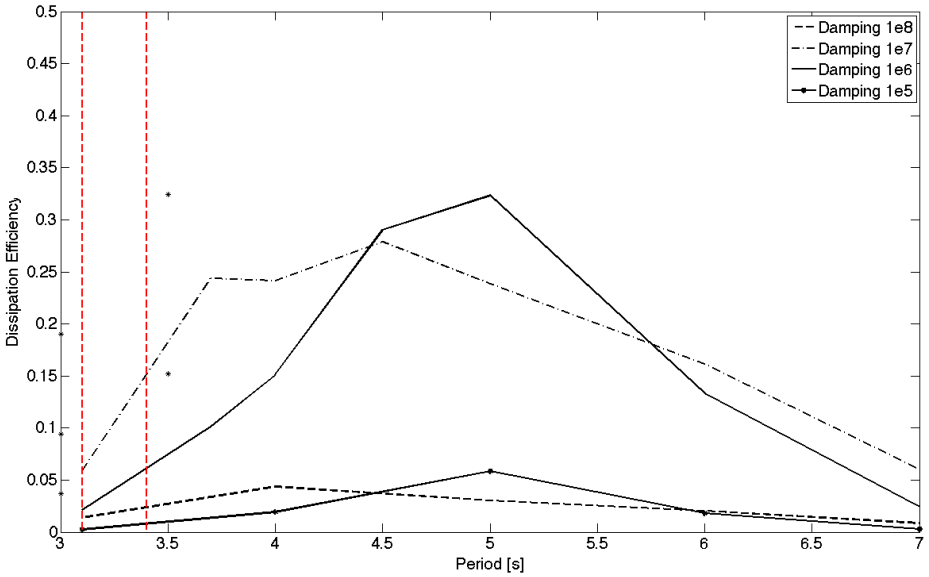

Figure A.4 *The resulting dissipation efficiency of investigation sample X20 for alternating wave period.*

Comparisons for all F2 samples with alternating ratio of wavelength per total structure width are shown in the following graphs. The resulting dissipation efficiencies are shown in *Figure A.5* and *Figure A.6* for a constant combined damping coefficient of 1e5 Ns/° and 1e7 Ns/° respectively.

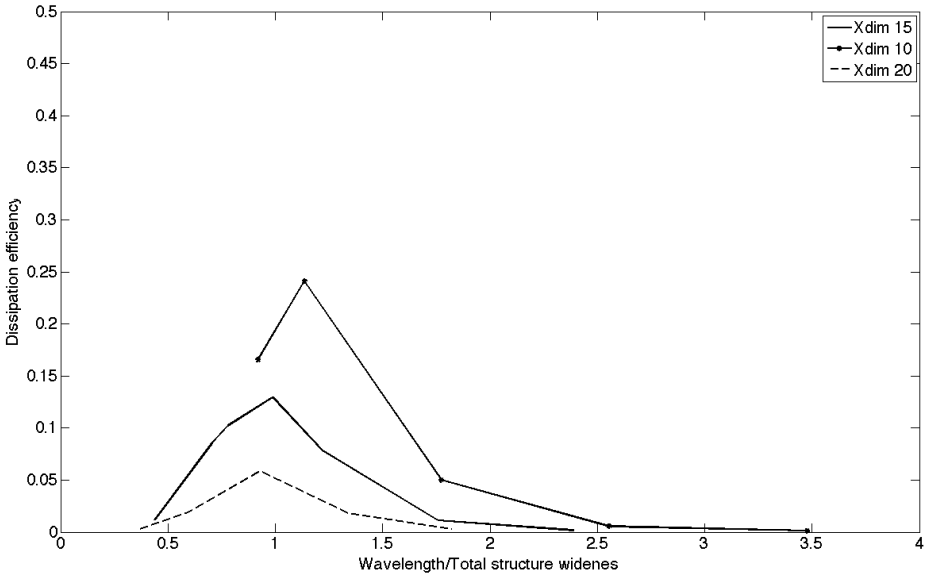

Figure A.5 *All F2 samples compared for alternating ratio of wavelength per total structure width. The resulting dissipation efficiencies are shown for a constant combined damping coefficient of 1e5 Ns/°.*

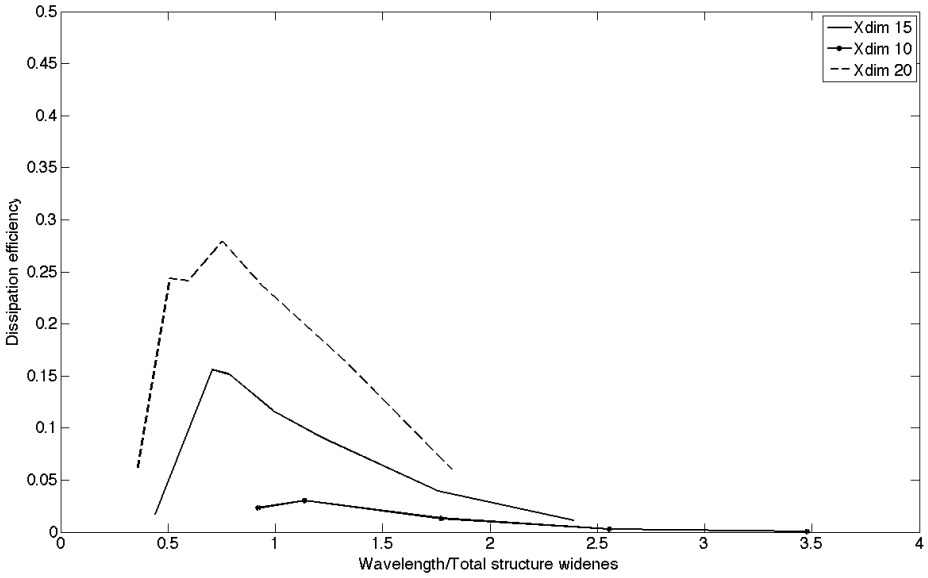

Figure A.6 *All F2 samples compared for alternating ratio of wavelength per total structure width. The resulting dissipation efficiencies are shown for a constant combined damping coefficient of 1e7 Ns/°.*

9 Appendix B

The graphs found in this appendix gather the simulation results of a sample included in investigation case M6. The sample presented here has a submerge area of 33%. *Figure B.1* and *Figure B.2* show the dissipation efficiency over combined damping coefficient and efficiency over wave period respectively. In the figures the energy dissipation efficiency is dimensionless, wave period in [s] and the combined damping coefficient is given in [Ns/°]. Peak efficiency of 30.4 % is found at a wave period of 5 seconds and a damping coefficient of 1 MNs/°.

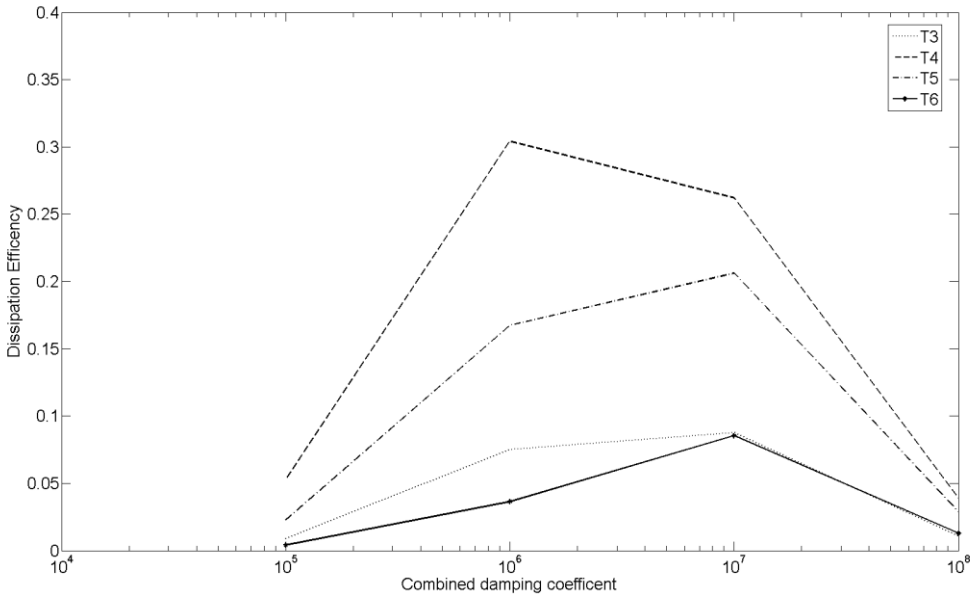

Figure B.1 *The resulting dissipation efficiency of investigation sample 33% for alternating combined damping coefficient.*

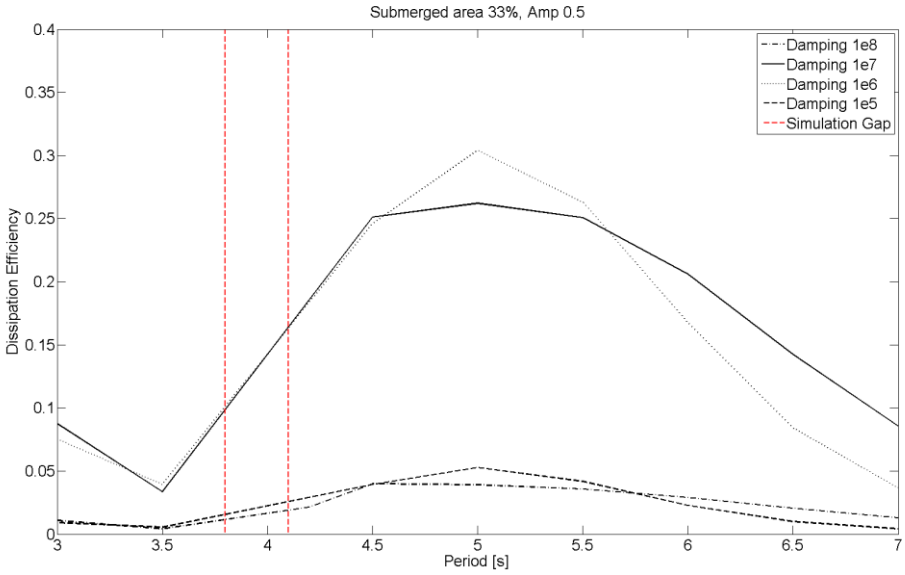

Figure B.2 *The resulting dissipation efficiency of investigation sample 33% for alternating wave period.*

The sample presented here has a submerge area of 66%. *Figure B.3* and *Figure B.4* show the dissipation efficiency over combined damping coefficient and efficiency over wave period respectively. In the figures, the energy dissipation efficiency is dimensionless, wave period in [s] and the combined damping coefficient is given in [Ns/°]. Peak efficiency of 33.3 % is found at a wave period of 5.5 seconds and a damping coefficient of 1 MNs/°.

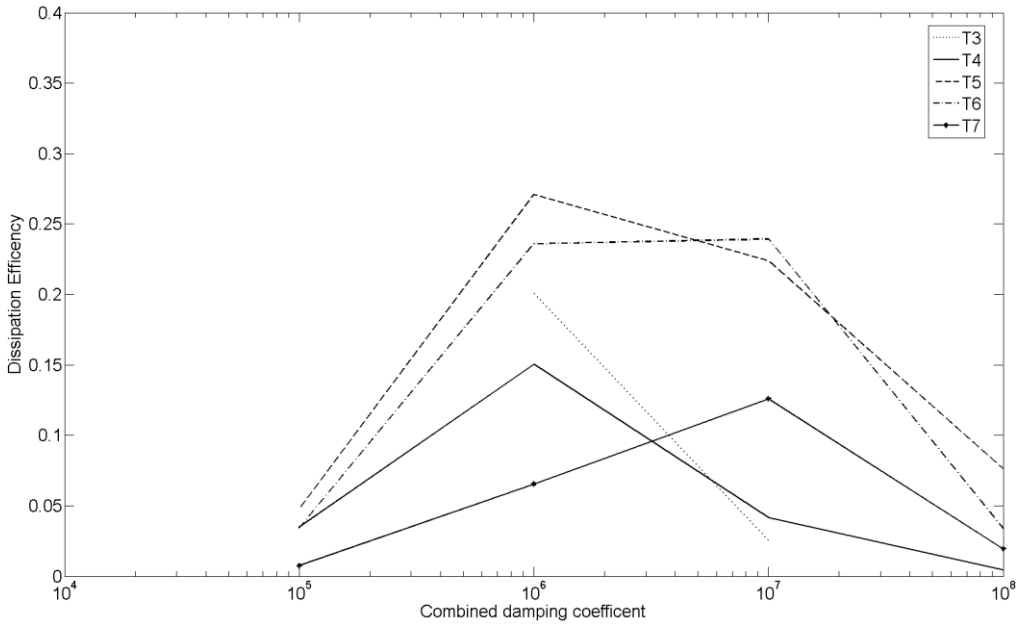

Figure B.3 The resulting dissipation efficiency of investigation sample 66% for alternating combined damping coefficient.

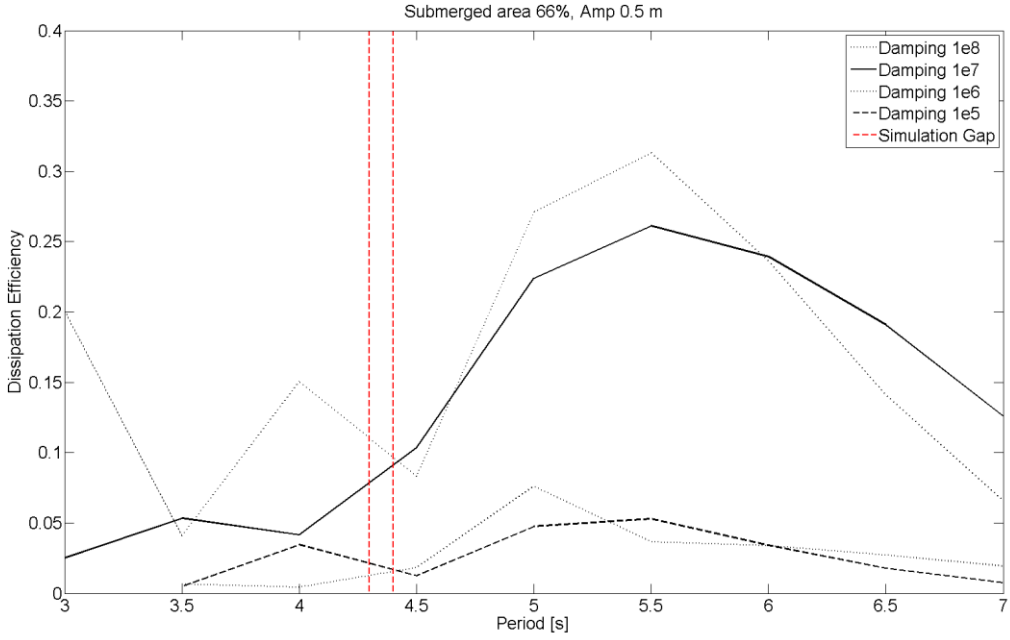

Figure B.4The resulting dissipation efficiency of investigation sample 66% for alternating wave period.